biomechanics

MDPI

Article

Development and Cross-Platform Benchmarking of an ArtiSynth Lower-Limb Gait Model Against OpenSim

Alexander Graf * and Wojciech Kowalczyk

Chair of Mechanics and Robotics, University of Duisburg-Essen, 47057 Duisburg, Germany; wojciech.kowalczyk@uni-due.de
* Correspondence: alexander.graf-lmr@uni-due.de; Tel.: +49-(0)-203-379-1265

Abstract

Background: In biomechanical research, combined simulation of multibody (MB) and finite element (FE) models enable the simultaneous study of global dynamics and tissue-level mechanics. Yet validated pipelines that bridge the MB and FE domains are often complicated and involve multiple software tools. ArtiSynth is an open-source Java-based biomechanical simulation framework for combined MB-FE simulations with forward and inverse simulation capabilities and FE contact modeling. It features an importer for OpenSim models to be used as foundation for combined MB-FE models. However, the performance of OpenSim models in the ArtiSynth environment has not been evaluated to this day. **Methods:** To address this gap, we developed an ArtiSynth lower-limb model based on an OpenSim model and evaluated it across multiple subjects and trials. Motion and force data from 100 trials of 30 adult healthy participants were processed and used in OpenSim and ArtiSynth inverse/forward computations. A representative trial was selected per participant using the SMaRT algorithm and pooled for Statistical Parametric Mapping (SPM, paired t-tests). **Results:** Albeit statistically significant differences in most evaluated features, the results showed great kinematic reproducibility (max RMS joint angle error of 2.81°. Partial kinetic agreement was observed (max RMS joint moment error of 0.49 N m kg^{-1}) and substantial differences in muscle recruitment (max RMS muscle force error of 262.48 N). Recommended physical plausibility thresholds for forward dynamics were violated approximately 90% of the time in both frameworks, indicating a limitation not unique to ArtiSynth. **Conclusions:** Although the current results are promising, future research is needed to reduce current residuals and improve muscle recruitment strategies in ArtiSynth before the model can serve as physiologically reliable foundation for combined MB-FE studies.

Keywords: musculoskeletal modeling; multibody dynamics; finite element analysis; lower-limb biomechanics; hybrid modeling

Check for updates

Academic Editor: Bernardo Innocenti

Received: 25 September 2026
Revised: 9 November 2026
Accepted: 10 November 2026
Published: 13 November 2026

Copyright: © 2026 by the authors. Licensee MDPI, Basel, Switzerland. This article is an open access article distributed under the terms and conditions of the Creative Commons Attribution (CC BY) license.

1. Introduction

In the field of biomechanics, numerical simulations have emerged over the last few decades as a standard tool to model and analyze the mechanics of biological systems [1]. Generally, these modeling techniques can be classified into finite element and multibody simulations [1]. Typically, MB simulations analyze (jointed) rigid systems to compute muscular and/or joint contact forces, commonly through inverse dynamics simulations. FE simulations target local stress and strain phenomena [2], contact between tissues and implants [3,4], as well as material nonlinearity [1,5]. They are also used to study remodeling processes of biological tissue, such as growth [6], to generate mesoscale structures of bone [7], or to capture degenerative processes [8–10].

However, in recent years, coupled MB-FE simulation approaches (including hybrid models and co-simulation methods) have been proposed that combine the strengths of both methods, as they provide a comprehensive view of the underlying biological system, considering both the overall kinematics and kinetics, as well as the inner state of the model tissue response [11]. Consequently, both simulation techniques have been used for a vast amount of biological structures during the last years, including the hip [12], spine [11,13,14], knee [15], and foot [16]. Coupled MB-FE simulations use two different software programs and follow either a unidirectional or a bidirectional approach [11,15]. In a unidirectional simulation, a multibody dynamics simulation is used first to estimate joint kinematics, moments, and muscle forces. These quantities then serve as boundary conditions for the finite element simulations that compute contact conditions, stresses, strain, etc. [17–20]. In a bidirectional setup, however, the finite element and multibody dynamics simulations run in a loop such that the calculated deformation is fed back into the multibody system to calculate updated muscle forces and secondary kinematics [15,21–24].

Contrary to that are several single-framework approaches, such as ReadySim [25] or ArtiSynth [26]. ArtiSynth 3.9 is an open-source, Java-based biomechanical simulation framework for combined simulation of rigid and flexible structures with forward and inverse capabilities, even if these structures are in contact [26]. ArtiSynth has a wide range of biomechanical applications [13,16,27–33] and features an OpenSim importer, with which existing OpenSim 4.5 models [34] can be imported to ArtiSynth. These models could act as potential baselines or foundations to build combined MB-FE models upon, thereby accelerating the currently labor-intensive step of model creation.

A benchmark is a standard tool for competitive evaluation and comparison of competing systems or components according to specific characteristics [35]. As such, benchmarks are common practice in computational modeling [36–38] to provide a computational reference for future models, sometimes even including reference solutions, and to evaluate the robustness of the applied methodologies [38]. From earlier computational comparisons, it is known that different modeling assumptions or software packages produce vastly different results when provided with the same biomechanical problem [39–42]. Therefore, the idea behind this study is, first, to build a functioning ArtiSynth model of an imported OpenSim gait model in the look and feel of OpenSim. Second, the inverse and forward computations of ArtiSynth are compared against the corresponding OpenSim output, which serves as gold standard for this comparison. It is assessed whether ArtiSynth reproduces those for a wide range of participants and trials in an implementation specific repducibility study. Statistically significant differences between both frameworks are expected, as shown by similar studies [41,42]; however, the amount of agreement decides whether the established model may serve as foundation for combined MB-FE simulations in the future. The archived ArtiSynth model and all accompanying code (including the additions to the artisynth core code) are publicly available under https://doi.org/10.5281/zenodo.24087589 (accessed 11 November 2026).

2. Materials and Methods

2.1. Motion Data Collection

Motion and force data were obtained from two multidisciplinary research projects [43,44]. The authors obtained Institutional Review Board approval for instrumental gait analysis and clinical examination from the Ethics Committee of the University Duisburg-Essen (application number 18.7988). Participants underwent a 3D gait analysis and a clinical examination. The gait analysis was performed using a Vicon 3D motion capture system with ten tracking cameras (100 Hz, Oxford Metrics Ltd., Oxford, UK), two video cameras (50 Hz, Basler AG, Ahrensburg, Germany) and two forceplates (1000 Hz, AMTI-OR6, Advanced Mechanical Technology Inc.,

Watertown, MA, USA). A full body Plug-in Gait marker set (Vicon Motion Systems Ltd., Oxford, UK) was attached to the participants legs, arms, trunk and head, with one additional marker at the tip of each hallux [45]. All subjects walked barefoot at a self-selected speed along a 10 m walkway. For each subject, the data of at least four trials with clear foot–forceplate contact were collected. All raw kinematic data were filtered with a Woltring filter.

From these collected data, we excluded all trials that did not meet our inclusion criteria (valid marker positions and corresponding ground reaction forces for all time steps). The remaining dataset contained 100 trials from 30 healthy subjects (11 males and 19 females; age: 56.00 ± 11.97 yr; height: 169.43 ± 9.22 cm; mass: 72.65 ± 12.77 kg) with no history of musculoskeletal disorders. During processing from .c3d to .trc, the time-averaged center of mass (CoM) displacement ($\bar{v}_{CoM} \cdot \Delta t$) in walking direction was obtained from the measured CoM trajectory and subtracted from all marker positions and force plate data (including center of pressure (CoP) information) in each trial. The ground reaction force (GRF) vectors and moments (GRM) about the center of pressure remained unchanged. This resulted in a treadmill-like movement done to stabilize tracking during ArtiSynth inverse simulations; however, the adjusted experimental data were fed to both simulation pipelines. Consistency of dynamic and kinematic data was verified in OpenSim and ArtiSynth separately by comparing CoP position, marker position and force magnitudes between adjusted and original data visually.

2.2. OpenSim Simulation Procedure

We used a publicly available adaptation [46] of the OpenSim model (Figure 1) developed by Hamner et al. [47], which features the Vicon Plug-in Gait (PiG) markerset [48]. Details of the model configuration are described there, but in short, the model consists of 12 segments, with 29 degrees of freedom (DoF). The lower extremity and back joints are driven by 92 Hill-type musculotendon actuators, and the arms are driven by torque actuators [47]. The subtalar and metatarsophalangeal joints were locked, which is common practice for models with feet modeled as single segments [49,50]. We adjusted this to our own experimental protocol by adding all missing experimental markers, including the hallux tip markers "LBTO" and "RBTO" and a "RBAK" marker, which served for posture identification [45]. Of the existing model markers, forearm markers were renamed from "LFRA" and "RFRA" to "LFRM" and "RFRM". "LFRM" and "RFRM" were detached from the ulna and re-attached to the radius, since the radius rotates around the ulna during pronation and supination.

We used static trials to scale the model for each participant according to the OpenSim documentation. Concretely, the generic model was scaled to the participants' anthropometry based on experimentally measured markers placed on anatomical landmarks. A virtual marker set was placed on the model based on these anatomical landmarks. Segments were then scaled such that the distances between the virtual markers matched the distances between the experimental markers. Mass and inertia tensors were adjusted accordingly. Left and right body segments were scaled uniformly and individually. Scaling weights were set to 1 after running a sensitivity analysis on them (Table S1). Details on the procedure can be found in Section S1.1 of the Supplementary Material [51].

After scaling the model, processed marker trajectories were imported into OpenSim 4.5. The segment poses corresponding to the marker trajectories were tracked using inverse kinematics (IK) analyses. Optimal marker weights were identified by formulating a bilevel optimization scheme (Section S1.2 of the Supplementary Material). In short, we defined a least-squares optimization problem (outer problem) to minimize the tracking root mean square (RMS) error associated with the IK run (inner problem) of the dynamic trial [52,53]. To reduce computational costs, markers were grouped by anatomical segments (Table S2) [54,55], and optimization was

performed on a subset of 10 arbitrarily selected trials, one per participant. IK was then re-run with the calibrated marker weights (Table S3) for all 100 trials, and the RMS of the calibration set and all trials were compared (Figure S1).

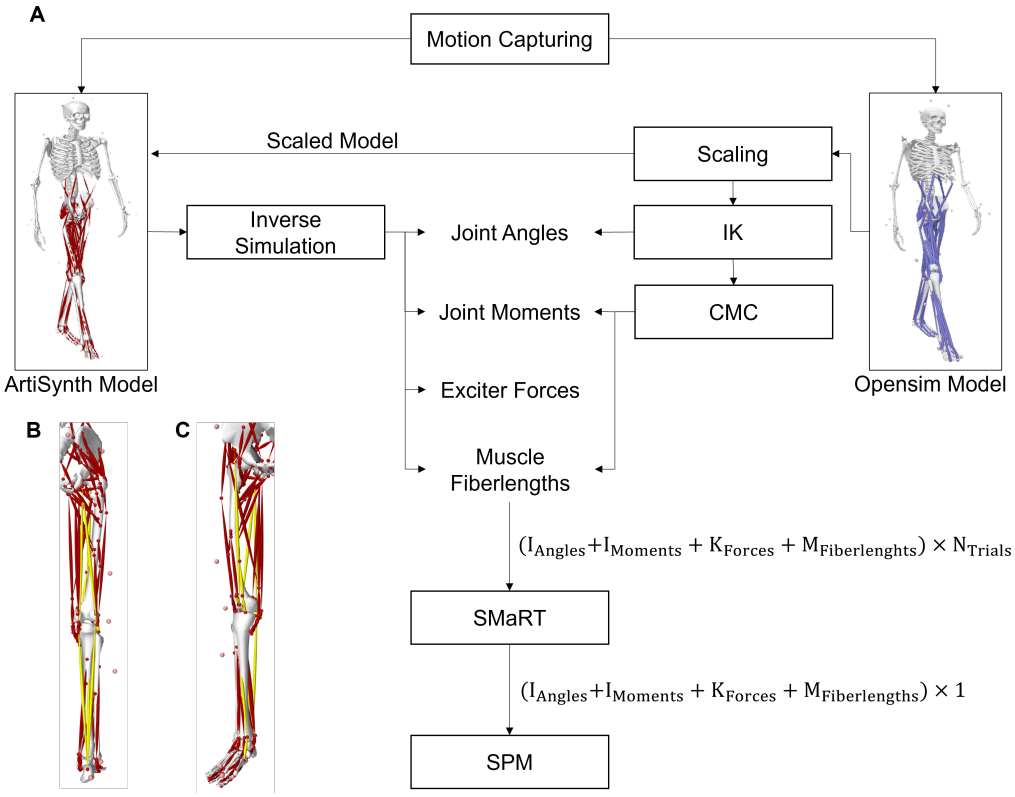


Figure 1. (**A**) The workflow of the study. All motion capturing trials were fed as input to OpenSim and ArtiSynth simulations that computed joint angles, moments, exciter forces, and muscle fiber lengths each. Per participant, these combined results were collected and passed to the SMaRT algorithm to select the representative trial per participant. The selected representative trials of all participants were then pooled for statistical parametric mapping. (**B**) Rear view of the right leg of the ArtiSynth model. (**C**) Frontal view of the right leg of the ArtiSynth model. Evaluated muscles are highlighted in yellow.

Although the residual reduction algorithm (RRA) is the default step between IK and muscle estimation [56], it was skipped here, since ArtiSynth does not provide a corresponding feature nor inverse dynamics (ID). So, for the sake of pipeline comparability, the compute muscle control (CMC) algorithm was used in two stages: 1. to compute joint moments by replacing the set of muscles with ideal joint exciters (commonly known and referred to in the following as reserve actuators) and 2. to estimate muscle forces by extending the set of muscles by said exciters. In short, CMC computes a set of desired generalized accelerations $\ddot{\vec{q}}^*$ to drive the model coordinates $\vec{q}$ towards experimental coordinates $\vec{q}_{exp}$ using PD control [57].

$$\ddot{\vec{q}}^*(t+\Delta t) = \ddot{\vec{q}}_{exp}(t+\Delta t) + \vec{k}_v\left[\dot{\vec{q}}_{exp}(t) - \dot{\vec{q}}(t)\right] + \vec{k}_p\left[\vec{q}_{exp}(t) - \vec{q}(t)\right] \quad (1)$$

Herein, $\vec{k}_v$ and $\vec{k}_p$ are feedback gains for velocity and position errors. CMC then computes each exciter control a_k such that it leads to a desired acceleration $\ddot{q}_i$ by minimizing

a cost function J. OpenSim features two formulations, called slow and fast target (see Section S1.3 of the Supplementary Material for more detail) [58].

$$\min_a J = \sum_k a_k^2 + \sum_i w_i(\ddot{q}_i^* - \ddot{q}_i)^2 \quad (2)$$

$$\min_a J = \sum_k a_k^2 \quad (3)$$

$$\text{subject to } \ddot{q}_i^* - \ddot{q}_i = 0 \qquad \forall i \quad (4)$$

The computed controls are then used in a forward dynamics simulation advancing the model in time by Δt. To compute pure joint moments (muscle forces excluded), fast optimization was set to "false" with a CMC time window of 1 ms, mirroring the CMC settings otherwise used in RRA [56]. Exciter settings and task set weights are based on OpenSim guidelines for RRA and shown in Table S4. Since the exciter set contained only reserve actuators, no constraints were defined [56].

To estimate muscle forces, fast optimization was set to "true" with a CMC time window of 10 ms [58]. Corresponding exciter settings and task set weights are according to OpenSim guidelines for CMC and also provided in Table S4. All muscle excitations were constrained to an interval of $[0.02, 1]$ during muscle-driven CMC. In both CMC setups, we applied GRF and GRM to both calcanei and defined GRF as point forces. We used a low frequency cut-off at 6 Hz and constant $K_p = 100$ and $K_v = 20$ values. Integrator and optimizer settings were defined according to OpenSim simulation guidelines with 30,000 max. integrator steps, step sizes between $[1 \times 10^{-8}, 1]$, and an integrator error tolerance of 1×10^{-5}. IPOPT run with 2000 max. optimizer iterations [58].

Since ArtiSynth tracks marker positions where CMC tracks joint angles, we added point kinematics analyses for each assigned model marker to the CMC setup files to compute the marker tracking error between model and experimental positions [59].

2.3. ArtiSynth Simulation Procedure

The scaled OpenSim models were imported into the latest development version of ArtiSynth, 3.9 (https://github.com/artisynth/artisynth_core, accessed on 9 November 2026) for each subject and trial (Figure 1). The left and right scapulae and clavicles have zero mass and a zero inertia tensor in the provided base model. As this posed a problem to the ArtiSynth solver, we assigned a negligible density of $1\,\mathrm{kg\,m^{-3}}$ to all four bones and recomputed the mass and inertia tensor based on that density in ArtiSynth. Thereby, we introduced a total of 1.6×10^{-4} kg to our system. Joint limits and lockings were formulated according to the OpenSim model.

ArtiSynth provides inverse solving capabilities to compute exciter activations a based on experimental motion data, conceptually similar to CMC [32,60]. However, where OpenSim tracks generalized coordinates (usually joint angles), ArtiSynth tracks experimental marker positions. The workflow does not require an inverse kinematics computation prior to solving for muscle activations, but we did so in order to provide achievable target positions and velocities for the model markers. Marker velocities were computed for every experimental marker trajectory and smoothed using a 4th-order Savitzky–Golay filter [61,62].

To solve for muscle excitations, desired accelerations $\ddot{\vec{x}}^*$ were computed first using PD control and then integrated over time.

$$\ddot{\vec{x}}^* = K_d\left[\dot{\vec{x}}_{exp}(t) - \dot{\vec{x}}(t)\right] + K_p\left[\vec{x}_{exp}(t) - \vec{x}(t)\right] \quad (5)$$

$$\dot{\vec{x}}^*(t + \Delta t) = \dot{\vec{x}}(t) + \Delta t \cdot \ddot{\vec{x}}^* \quad (6)$$

The scalar PD controller gains for position (K_p) and velocity (K_d) were computed according to ArtiSynth guidelines [60]. However the model overshot extensively with the default value of K_d, so Equation (8) was modified.

$$K_p = \frac{1}{\Delta t T} \quad \Rightarrow [K_p] = \mathrm{s}^{-2} \tag{7}$$

$$K_d = \frac{0.1}{\Delta t}\text{, instead of } K_d = \frac{1}{\Delta t} \quad \Rightarrow [K_d] = \mathrm{s}^{-1} \tag{8}$$

T is called chase time, with $T \geq \Delta t$, depending on how much the system tends to overshoot. ArtiSynth then computes exciter controls $\vec{a}$ to achieve $\dot{\vec{x}}^*$ by minimizing a cost function J. The optimization problem may be customized by adding predefined cost or constraint terms, including motion targets (i.e., tracking error), Equation (9); regularization, Equation (10); and excitation damping, Equation (11) [60].

$$\phi(m) = \frac{1}{2} w_m \sum_i \left[W_{m,ii} \left(\dot{\tilde{x}}_i(t) - \sum_k H_{m,ik} a_k \right) \right]^2 \text{ with } \dot{\tilde{x}}_i = \dot{x}_i^* - \dot{x}_{0,i} \tag{9}$$

$$\phi(a) = \frac{1}{2} w_a \sum_k W_{a,kk} a_k^2 \tag{10}$$

$$\phi(d) = \frac{1}{2} w_d \sum_k \frac{1}{\Delta t^2} \left(W_{a,kk} a_k^2 - 2 a_{0,k} W_{a,kk} a_k \right) \tag{11}$$

Herein, $w_{m,a,d}$ are weights associated with each cost term, W_m is a diagonal matrix containing the individual weight assigned to each marker i, H_m is a motion excitation response matrix [32]. $\dot{\vec{x}}_0$ denotes the velocity vector at $\vec{a} = 0$. W_a is a diagonal weight matrix indicating the relative importance of each exciter k. By default, ArtiSynth normalizes its cost terms, making $w_{m,a,d}$, H_m and $W_{m,a}$ all relative to each other. Also, ArtiSynth offers to reformulate the cost function in terms of excitation changes Δa_k if exciter forces are not linear with respect to the excitations, as are Hill-type equilibrium muscle models [60].

For this study, we added Equation (9) and Equations (10) and (11) in two setups. To compute joint moments, we formulated tracking error as part of the cost function, Equation (12), thereby mimicking the slow target formulation of OpenSim. To also compute muscle forces, we introduced tracking via equality constraints, Equation (15), which is conceptually similar to OpenSim's fast target formulation. We chose to include excitation damping as a cost term there, since ArtiSynth does not feature the natural damping provided by the activation dynamics of the underlying Hill-type muscle model. Incremental computation was set to true, as this resulted in more stable simulations for all investigated trials [58,60].

$$\min_{\Delta a} J = \frac{w_m}{2} \sum_i \left[W_{m,ii} \left(\dot{\tilde{x}}_i(t) - \sum_k H_{m,ik} \Delta a_k \right) \right]^2 + \frac{w_a}{2} \sum_k W_{a,kk} \left(\Delta a_k^2 + 2 a_{0,k} \Delta a_k \right) \tag{12}$$

$$a_k = a_{0,k} + \Delta a_k \tag{13}$$

$$\text{subject to } a_{min,k} - a_{0,k} \leq \Delta a_k \leq a_{max,k} - a_{0,k} \tag{14}$$

$$\min_{\Delta a} J = \frac{w_a}{2} \sum_k W_{a,kk} \left(\Delta a_k^2 + 2 a_{0,k} \Delta a_k \right) + \frac{w_d}{2} \sum_k \frac{1}{\Delta t^2} W_{a,kk} \Delta a_k^2 \tag{15}$$

$$\text{subject to } \dot{\tilde{x}}_i(t) - \sum_k H_{m,ik} \Delta a_k = 0 \qquad \forall i \tag{16}$$

$$a_{min,k} - a_{0,k} \leq \Delta a_k \leq a_{max,k} - a_{0,k} \tag{17}$$

To replicate the reserve actuators in OpenSim, a custom "JointActuator" (JA) class was written, which has now been included in ArtiSynth's codebase. These exciters can be recruited by the controller alongside the model muscles in case the latter cannot produce the necessary torque to drive the model. The class utilizes the built-in function of ArtiSynth

to access and manipulate the individual DoF of any "Joint" class or its subclasses. This also includes the application of a force to a single DoF (or wrench to multiple DoFs in more general terms). All exciter components share an excitation and a maximum force property, where the applied force of an exciter at time t is computed by the current excitation value times its maximum force:

$$f_t = a_t \cdot f_{max} \tag{18}$$

The excitation of a JA is bounded to an interval of $[-1, 1]$ but can be adjusted externally to the class. Every JA is linked to a DoF of a joint and applies a force or torque to the DoF of that joint for every time step during simulation that corresponds to the computed excitation of the controller times its maximum force. We defined one JA per DoF for each joint, with a maximum force/moment of 1000 N/Nm in the lower limbs and 100 Nm in the upper limbs. Similarly to the OpenSim procedure to compute joint moments, JAs replaced the model muscles with an assigned weight of 1, so W_a becomes the identity matrix. In this setup, each DoF is driven by exactly one exciter, so the only redundancies to handle are joint limits (including the locked joints). The regularization term weight w_a was therefore set to its default value of $w_a = 1 \times 10^{-4}$. Stable simulations were achieved for T set to 1 ms.

To compute muscle forces, JAs extended the model muscles. To discourage the optimizer from recruiting the lower limb JAs, we screened their recruitment sensitivity with the subset of 10 arbitrarily selected trials already used to identify IK marker weights. The screening is described in more detail in Section S1.4 of the Supplementary Material. In short, the screening evaluated a grid spanning different JA to muscle-weight ratios and w_a values. If tracking is applied via equality constraints, then desired activation changes depend on the ratio between $w_{a,d}$ and Δt (Equations (S4)–(S11) in the Supplementary Material), while the exciter weights determine how the activations are distributed. However, depending on the chosen settings, the solver failed to find a feasible solution that satisfied the equality constraints for certain time steps and trials. We therefore added a fallback to use Equation (12) plus an additional excitation damping term due to the muscles being present, instead of Equation (15) for failed time steps. If the solver succeeded with the cost terms, then the next time step solve was attempted using Equation (15) again. The screening, therefore, also accounted for enabling stable simulations in fallback mode by varying w_m. JA-to-muscle-weight ratio was varied between 1, 1×10^3 and 1×10^6. We selected w_a such that the balance between regularization and excitation damping is evenly spaced between 0 and 1, at 0.2, 0.4, 0.6 and 0.8. w_m was scaled from 1 to 0.1 and 0.01. The screening results are provided in Figures S2 and S3; finally, we assigned a weight of 1 to all muscles and 10^6 to all lower-limb JAs, with $w_a = 15.0$ and $w_m = 0.01$. T was set to 10 ms in the muscle-driven simulations.

Experimental ground reaction forces and moments were applied directly to both calcanei using the resulting forces F and moments T derived from the force plates, as well as the moment introduced by the distance s between the CoP and the origins of the local coordinate system of the calcanei [63].

$$\vec{M}_c = \vec{s} \times \vec{F} + \vec{T} \tag{19}$$

We used default integrator and solver settings for inverse simulation, full backward Euler integrator with global stiffness stabilization. Hybrid solves were disabled, as they do not work well with the inverse solver [60]. Gravity was defined with $-9.81\,\mathrm{m\,s^{-2}}$ in negative y-direction. Coefficients for inertial damping properties were set to 1.

2.4. Benchmark Criteria and Data Analysis

We defined several criteria to assess: (1) physical/biomechanical plausibility of the simulations and (2) the amount of agreement between the two modeling platforms on

(ideally) the same problem. Plausibility can be expressed in terms of tracking error [64] and residual magnitude [64,65], i.e., model divergence from experimentally measured ground truth. Comparative criteria between model versions or modeling platforms specifically address kinematic, kinetic, and muscle tendon unit (MTU) agreement [39–41,64,66–68]. There is a number of different approaches: applying statistical tests to peak values [40], reporting error measures such as standard error of measurement (SEM) [67] or root mean square error (RMS) [40,41,69], or waveform analyses, especially statistical parametric mapping (SPM) [40,41,67]. A detailed list of provided criteria and thresholds for acceptance is presented in Table 1.

Table 1. Criteria and corresponding thresholds used in this comparative study.

#	Criterion	Threshold
1	tracking agreement	Mean marker tracking RMS error ≤20 mm [64]
2	kinematic agreement	RMS of each joint angle ≤2° [66]
3	kinetic agreement	Residuals 3a–c below the thresholds defined by [65]
3a	zero moment point (ZMP)	Distance between ZMP and CoP ≤ 5 cm
3b	ZMP free moment	≤10% of peak magnitude of experimental GRF free moment
3c	total ext. forces	≤5 %(F_y) and ≤10 %($F_{x,y}$) of peak magnitude of experimental GRF
4	waveform agreement	Number and amount of statistically significant differences [41,68]
5	MTU agreement	Reserve actuator recruitment ≤5% of net joint moment [64]

According to the defined criteria, we compared tracking errors, joint angles and moments, muscle forces and normalized fiber lengths, and reserve actuator recruitment for all computations of all remaining trials not used for screening or calibration (90 trials, originating from 28 participants). The time domain of all data was normalized to a gait cycle duration of 100%, ranging from foot strike to foot strike. Pelvic angles were derived from the orientation of the progression frame, as described by [48]. All joint moments were normalized to body mass. Muscle fiber lengths were normalized to the optimal fiber length of the underlying Hill-Type muscle model [70]. Since this study focuses on gait, the comparison is limited to the pelvis, hip, knee, and ankle joints, as well as selected muscles that have shown to play a significant role in gait [57,71–73]: rectus femoris (RF), biceps femoris (BF), gastrocnemius lateralis (GL) and medialis (GM), vastus medialis (VM), semimembranosus (SM), and soleus (SOL) (Figure 1).

Since the number of contributed trials per participant varies, a representative trial must be found for each participant. The results consisting of I joint angles and moments and K exciter forces (muscles plus reserve actuators) and M fiber lengths of N trials are collected per participant (Figure 1). Collected results were imported into MATLAB R2025a (MathWorks, Inc., Natick, MA, USA) for further processing. Since the time domain is normalized to 101 data points, the resulting dataset has the dimensions $101 \times (2I + K + M) \times N$. To account for different feature magnitudes, each feature was standardized using z-scores across trials [74]. The standardized dataset is passed to the "Selection Method for a Representative Trial" (SMaRT) algorithm [75], which returns the representative dataset for each participant in the dimensions $101 \times (2I + K + M) \times 1$ using principal component analysis (PCA). Due to simulation differences, selected representative trials varied for ArtiSynth and OpenSim simulations. To enforce the selection of the same trials, the OpenSim dataset served as reference for selection, and the same trials were selected in the ArtiSynth dataset accordingly. We then performed SPM-based paired t-tests ($\alpha = 0.05$) for each of the $2I + K + M$ features [76]. Uncertainties of each investigated feature were obtained using 95% bias-corrected and accelerated (BCa) bootstrap confidence intervals [77].

3. Results

Due to the vast amount of generated data, the following paragraphs will be limited to the comparison of global model behaviors in the sagittal plane. We provide complete results for every investigated feature in the supplementary material. The simulations showed that, throughout inverse kinematics and both forward dynamics setups, criterion 1 was not achievable for a variable amount of trials. Specifically, 11 out of all 100 trials, or 9 out of 90 evaluated trials, were above a tracking RMS error of 20 mm (Table S5). A total of 31 of 90 evaluated trials entered fallback, and in those trials, 12.90% of the time steps were solved in fallback. Tracking RMS error did not scale with the percentage of time steps being solved via fallback (Figure S4). On average, the trials entering fallback gained 2.76 ± 0.90 mm of tracking error compared to inverse kinematics.

3.1. Kinematics

The mean marker tracking RMS error during IK was 13.59 ± 3.49 mm for ArtiSynth and 13.41 ± 3.20 mm for OpenSim (Figure 2, left). If muscle forces were excluded during forward dynamics, the mean marker tracking error was 13.89 ± 3.94 mm for ArtiSynth and 14.21 ± 3.10 mm for OpenSim, respectively (Figure 2, center). Including the muscle forces into forward dynamics produced a marker tracking error of 16.24 ± 3.17 mm for ArtiSynth and 13.53 ± 3.18 mm for OpenSim (Figure 2, right).

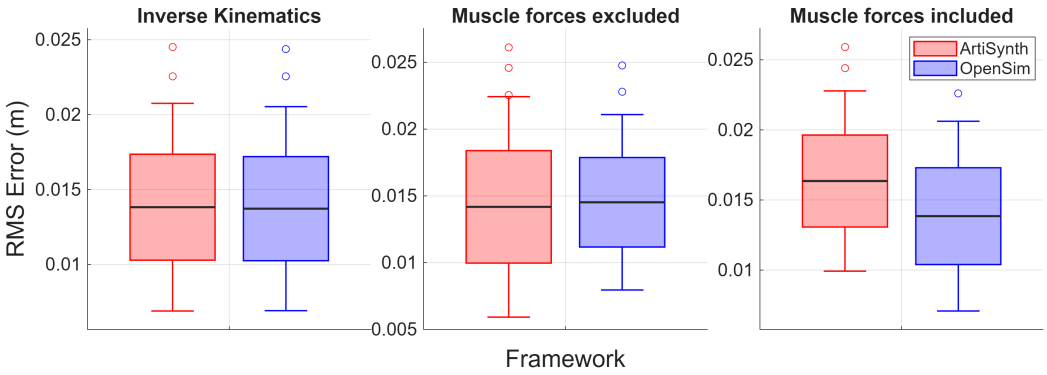


Figure 2. Computed marker tracking RMS error across all three simulation setups for 28 representative trials. IK computations (**left**), forward dynamics with excluded muscle forces (**center**) and forward dynamics with muscle forces included (**right**). Boxes are plotted as mean ± SD, whiskers extending to ±2SD and outliers beyond that.

Processed data from IK computations of 28 representative trials matched closely across all joints, despite statistically significant differences in every joint angle (Figures 3 and S5). Computed RMS values of all joint angles varied between 0.08° (pelvic rotation) and 0.37° (knee flexion), with corresponding coefficients of determination between 0.99 and 1.00 (Figure S6). Similarly, joint angles from FD, excluding muscle forces, align well, with similar statistically significant differences across all joints (Figure S7). The RMS error is between 0.18° (pelvic rotation) and 0.99° (ankle dorsiflexion), with corresponding coefficients of determination ranging from 0.99 (ankle dorsiflexion) to 1.00 (pelvic tilt, hip and knee flexion, Figure S8). When muscle forces were included in the simulations, statistically significant differences remain (Figure S9), with RMS errors between 0.40° (pelvic tilt) and 2.81° (knee flexion, Figure S10). Corresponding coefficients of determination span from 0.94 (ankle dorsiflexion) to 1.00 (pelvic tilt). The 95 % BCa confidence intervals further support close kinematic agreement during IK and muscle-excluded FD, as all upper confidence bounds remained below the predefined threshold of 2° (Table 2). During muscle-driven FD, knee flexion exceeded this threshold [2.66°, 3.00°]. In contrast, the intervals for hip flexion and ankle dorsiflexion included the threshold but remain inconclusive.

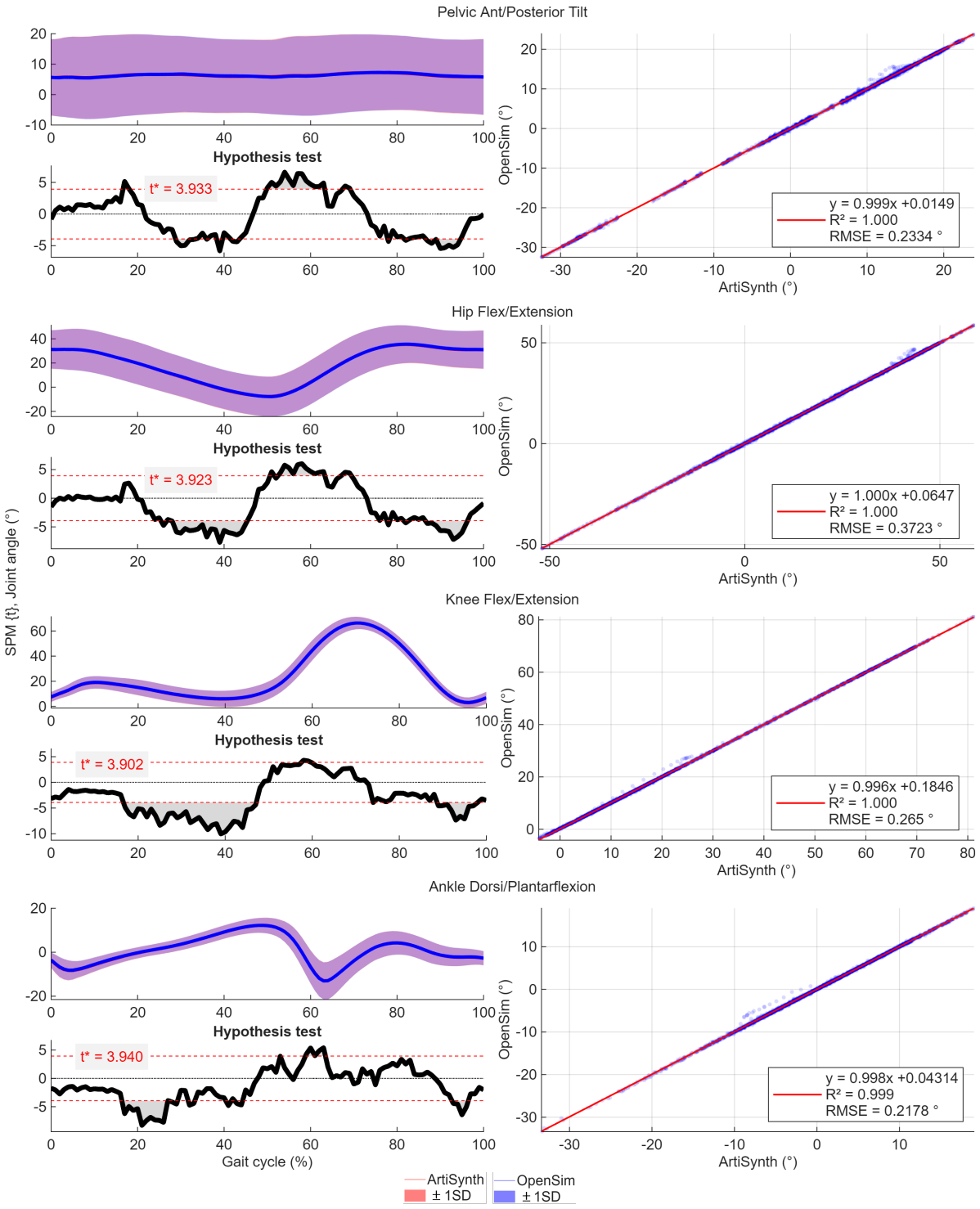


Figure 3. Joint angle SPM (**left**) and RMS (**right**) of IK computations from OpenSim (blue) and ArtiSynth (red). Each curve represents the average of 28 representative trials ± one standard deviation. All tests were performed with $\alpha = 0.05$ on 28 representative trials. Suprathresholds are indicated by t^* for every test. RMS were fitted linearly; identity is indicated as gray dashed line.

Table 2. Investigated feature uncertainties, quantified as 95% bias-corrected and accelerated (BCa) bootstrap confidence intervals.

Feature	**Inverse Kinematics**		**FD (Muscles Excluded)**		**FD (Muscles Included)**	
Joint Angles [°]	**RMSE**	**95% BCa CI**	**RMSE**	**95% BCa CI**	**RMSE**	**95% BCa CI**
Pelvic Ant/Posterior Tilt	0.23	[0.18, 0.35]	0.69	[0.20, 1.63]	0.40	[0.32, 0.53]
Pelvic Obliquity	0.22	[0.13, 0.43]	0.41	[0.18, 0.85]	0.75	[0.66, 0.85]
Pelvic Int/External Rotation	0.08	[0.07, 0.09]	0.18	[0.11, 0.35]	0.59	[0.52, 0.73]
Hip Flex/Extension	0.37	[0.28, 0.59]	0.94	[0.40, 1.93]	2.07	[1.96, 2.24]
Hip Ad/Abduction	0.19	[0.14, 0.33]	0.50	[0.27, 0.99]	1.13	[1.02, 1.29]
Hip Int/External Rotation	0.22	[0.15, 0.38]	0.53	[0.38, 0.87]	0.86	[0.78, 0.93]
Knee Flex/Extension	0.26	[0.18, 0.46]	0.52	[0.44, 0.74]	2.81	[2.66, 3.00]
Ankle Dorsi/Plantarflexion	0.22	[0.12, 0.42]	0.97	[0.83, 1.18]	1.99	[1.83, 2.17]
Reserve Actuator moment [N m kg^{-1}]						
Pelvic Ant/Posterior Tilt	-	-	0.49	[0.46, 0.56]	0.57	[0.54, 0.61]
Pelvic Obliquity	-	-	0.19	[0.16, 0.24]	0.19	[0.18, 0.21]
Pelvic Int/External Rotation	-	-	0.12	[0.08, 0.20]	0.08	[0.07, 0.11]
Hip Flex/Extension	-	-	0.16	[0.14, 0.19]	0.05	[0.04, 0.08]
Hip Ad/Abduction	-	-	0.11	[0.09, 0.13]	0.03	[0.02, 0.04]
Hip Int/External Rotation	-	-	0.02	[0.02, 0.03]	0.02	[0.01, 0.03]
Knee Flex/Extension	-	-	0.09	[0.08, 0.09]	0.11	[0.07, 0.18]
Ankle Dorsi/Plantarflexion	-	-	0.07	[0.06, 0.08]	0.04	[0.03, 0.05]
Muscle forces [N]						
M Rect Fem	-	-	-	-	208.36	[184.00, 251.99]
M Semimembranosus	-	-	-	-	187.76	[166.39, 208.29]
M Biceps fem long	-	-	-	-	73.07	[60.06, 94.34]
M Vas med	-	-	-	-	101.33	[86.56, 120.58]
M Gas lat	-	-	-	-	62.10	[54.70, 71.66]
M Gas med	-	-	-	-	262.48	[242.83, 279.70]
M Soleus	-	-	-	-	242.22	[217.34, 273.48]
Normalized fiber length						
M Rect Fem	-	-	-	-	0.13	[0.12, 0.13]
M Semimembranosus	-	-	-	-	0.04	[0.04, 0.05]
M Biceps fem long	-	-	-	-	0.03	[0.03, 0.03]
M Vas med	-	-	-	-	0.14	[0.14, 0.15]
M Gas lat	-	-	-	-	0.04	[0.04, 0.05]
M Gas med	-	-	-	-	0.05	[0.05, 0.05]
M Soleus	-	-	-	-	0.03	[0.03, 0.04]

3.2. Forward Dynamics with Excluded Muscles

Statistically significant differences in the computed joint moments during muscle-excluded FD were found across all joints, except for pelvis obliquity and rotation moments (Figure S11). Pelvic tilt, hip, and knee flexion moments are characterized by a larger transient in ArtiSynth simulations (Figure 4). Computed RMS errors ranged between 0.02 N m kg^{-1} (hip rotation moment) and 0.49 N m kg^{-1} (pelvic tilt moment), with corresponding coefficients of determination from 0.09 (pelvic rotation) to 0.99 (ankle dorsiflexion, Figure S12). Here, it should be noted that RMS errors and coefficients of determination regarding pelvis joint DoFs are distorted by the large transient in ArtiSynth, leading to small joint moment values being mapped onto the larger ones from ArtiSynth during the first 5–10% of the gait cycle. Confidence intervals of computed joint moments varied extensively (Table 2). While the ankle dorsiflexion moment CI is comparatively narrow [0.06 N m kg^{-1}, 0.08 N m kg^{-1}], the pelvic tilt moment exhibited the largest discrepancy [0.46 N m kg^{-1}, 0.56 N m kg^{-1}].

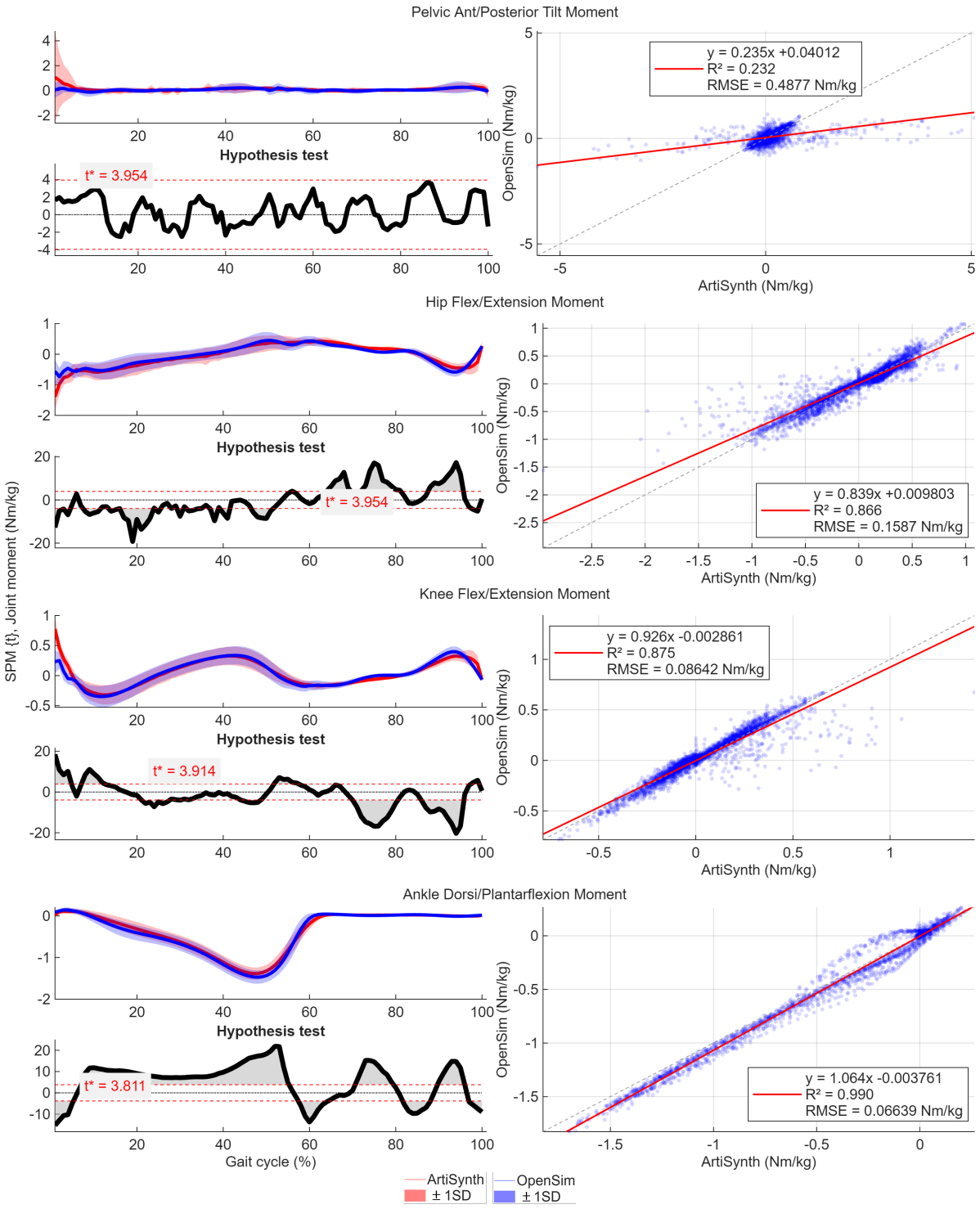


Figure 4. Joint moment SPM (**left**) and RMS (**right**) during FD with muscle forces excluded, from OpenSim (blue) and ArtiSynth computations (red). Each curve represents the average of 28 representative trials ± one standard deviation. All tests were performed with $\alpha = 0.05$ on 28 representative trials. Suprathresholds are indicated by t^* for every test. RMS were fitted linearly; identity is indicated as gray dashed line.

The kinetic guidelines 3a–c were generally violated across the entire time domain in all simulations, independent of the framework (Table 3). On average, guideline 3a was met quite often, in approximately 80 % of all time steps. A snapshot from one exemplary representative trial underlines the transient behavior in FD computations in ArtiSynth v.s. OpenSim (Figure S13). Once the transient phase is over, ZMP and CoP positions align fairly

well. However, criterion 3b is violated approximately 75 % of the time, while criterion 3c is violated roughly 85% of the time. Interestingly, residuals in the F_x-direction were met at 90% of time frames in OpenSim, compared to only 40% in ArtiSynth. On the other hand, F_y-direction residuals were met more often in ArtiSynth (80 % of the time), but not as often in OpenSim (65% of the time).

Table 3. Mean percentage of time steps violating the kinetic guidelines 3a–c according to [65], ±SD of the 28 representative trials. Note that guideline violations address physical reasonability as deviation from experimental data, not framework performance in itself.

Analysis	ZMP	Free Moment	Force	F_x	F_y	F_z	Any
FD with muscles excluded							
ArtiSynth	22.70 ± 19.38	74.68 ± 9.43	86.85 ± 7.23	61.78 ± 15.36	19.55 ± 10.83	69.59 ± 11.37	94.20 ± 5.50
OpenSim	22.88 ± 7.97	72.45 ± 7.81	81.22 ± 9.78	9.48 ± 12.22	34.02 ± 5.97	71.29 ± 11.69	92.96 ± 5.21
FD with muscles included							
ArtiSynth	20.05 ± 7.52	77.02 ± 7.82	84.30 ± 7.60	61.46 ± 12.56	15.84 ± 5.80	65.66 ± 10.21	94.55 ± 4.88
OpenSim	22.60 ± 10.34	73.80 ± 8.66	92.22 ± 5.37	71.00 ± 12.84	33.70 ± 6.79	70.33 ± 11.32	96.32 ± 3.12

3.3. Forward Dynamics with Included Muscles

Muscle recruitment of 28 representative trials diverged extensively between both frameworks (Figure 5). BF, GL, and SOL muscle forces are similar in shape and excitation timing, but statistically significant differences are observed for every muscle in the model (Figure S14). Moreover, RF, SM, and VM feature entirely different excitation curves in both frameworks. Corresponding RMS errors range from 62.10 N (GL) to 262.48 N (GM), with coefficients of determination between 0.07 (VM) and 0.82 (SOL) (Figure S15). All observed normalized fiber lengths align well with one another (Figure 6). However, statistically significant differences were found for all computed normalized fiber lengths (Figure S16). Interestingly, normalized fiber lengths of RF and VM differed by approximately 40% in value between 60 and 80% of the gait cycle, indicating a distinctly different muscle movement between both frameworks. Computed RMS errors are between 0.03 (BF) and 0.14 (VM), with coefficients of determination between 0.89 (SOL) and 0.99 (BF, Figure S17). The confidence intervals further support the substantial between-platform discrepancies in muscle force estimates. For example, GM and SOL exhibited CIs of [242.83 N, 279.70 N] and [217.34 N, 273.48 N], respectively. In comparison, normalized fiber lengths exhibited smaller RMSEs with comparatively narrow confidence intervals (Table 2).

Reserve actuators were recruited similarly across pelvic joints. Also, recruitment seemed to be adequately penalized in both frameworks, except between 60 and 80% of the gait cycle, during which all reserve actuators were recruited in ArtiSynth (Figure S18). Statistically significant differences were found in all joints, except for those reserve actuators supporting pelvic obliquity and rotation. The lowest RMS error was generated during hip rotation support with 0.02 N m kg^{-1}, while the highest was during pelvis tilt support at 0.57 N m kg^{-1} (Figure S19). The coefficients of determination range from 0.00 (knee flexion support) to 0.30 (pelvic obliquity support). The confidence intervals computed for RMSEs between different reserve actuator recruitments showed considerable variation (Table 2). The largest CI is observed for pelvic tilt support [0.54 N m kg^{-1}, 0.61 N m kg^{-1}], while the lowest and smalles CI is shown by hip rotation support [0.01 N m kg^{-1}, 0.03 N m kg^{-1}].

The violation of the kinetic guidelines 3a–c did not change significantly if muscles were included in forward dynamics simulations, with over 90% of time steps behaving physically unreasonably (Table 3). Guideline 3a was still met most of the time (approximately 80%), followed by the guidelines 3b and 3c in that order. While the guideline violation was similar to muscle-excluded simulations in ArtiSynth, violation of guideline 3c in the F_x-direction rose by 60% in OpenSim.

In ArtiSynth, the joint moment contribution from reserve actuators ranged from 2% (ankle dorsiflexion) to 15% (knee flexion) compared to the computed net joint moment (Figure 7). On the other hand, reserve actuator recruitment was adequately penalized by the OpenSim solver, where reserve actuators accounted for 0 (hip and knee flexion) to 5% (hip rotation) of the net joint moment. Pelvis joint moments were unaffected, since they contribute residuals to stabilize the model in space. On average, criterion 5 was violated by two of five reserve actuators in ArtiSynth, while it was entirely met in OpenSim.

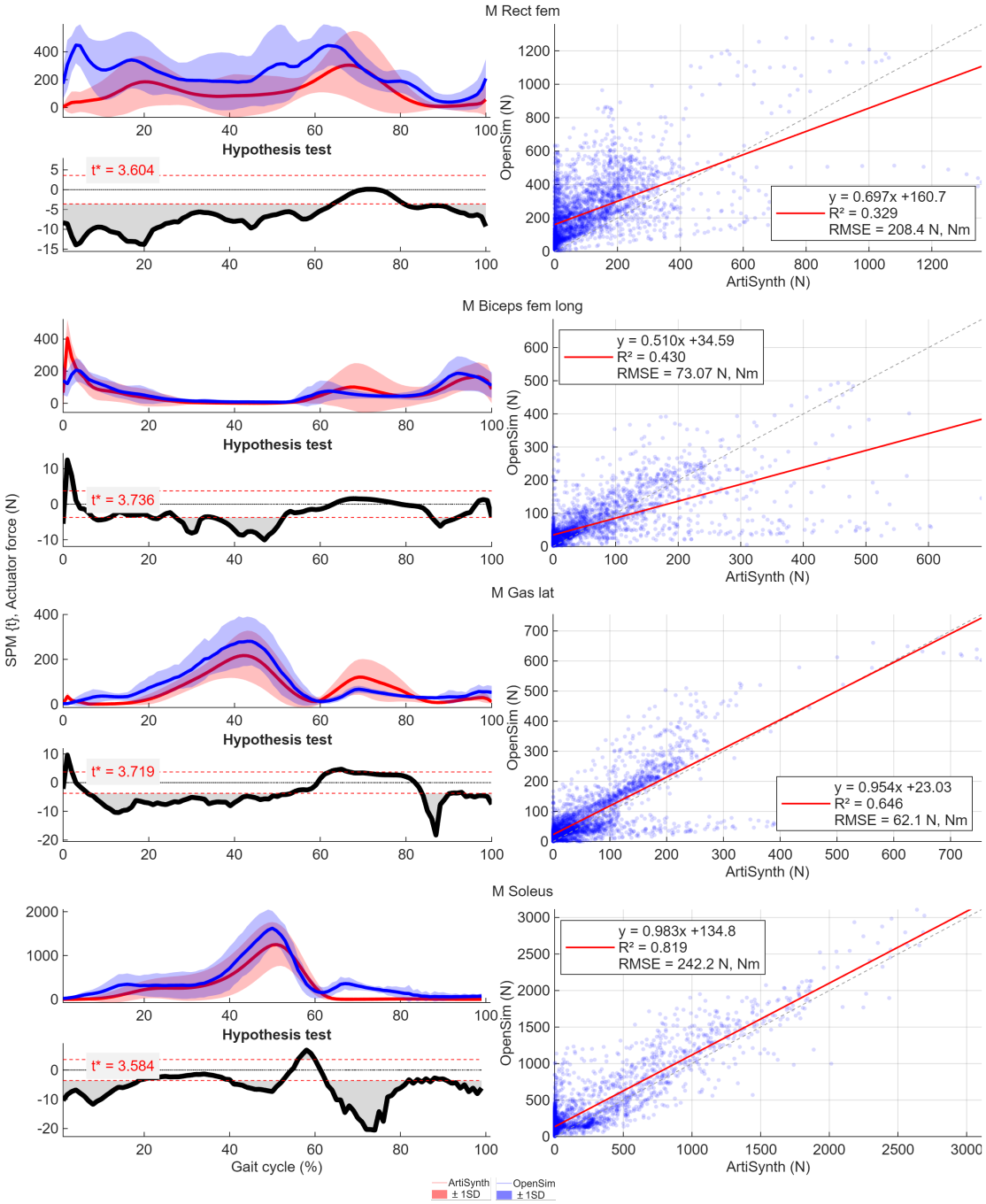


Figure 5. Computed muscle force SPM (**left**) and RMS (**right**) during FD from OpenSim computations (blue) and ArtiSynth computations (red). Each curve represents the average of 28 representative trials ± one standard deviation. All tests were performed with $\alpha = 0.05$ on 28 representative trials. Suprathresholds are indicated by t^* for every test. RMS were fitted linearly; identity is indicated as gray dashed line.

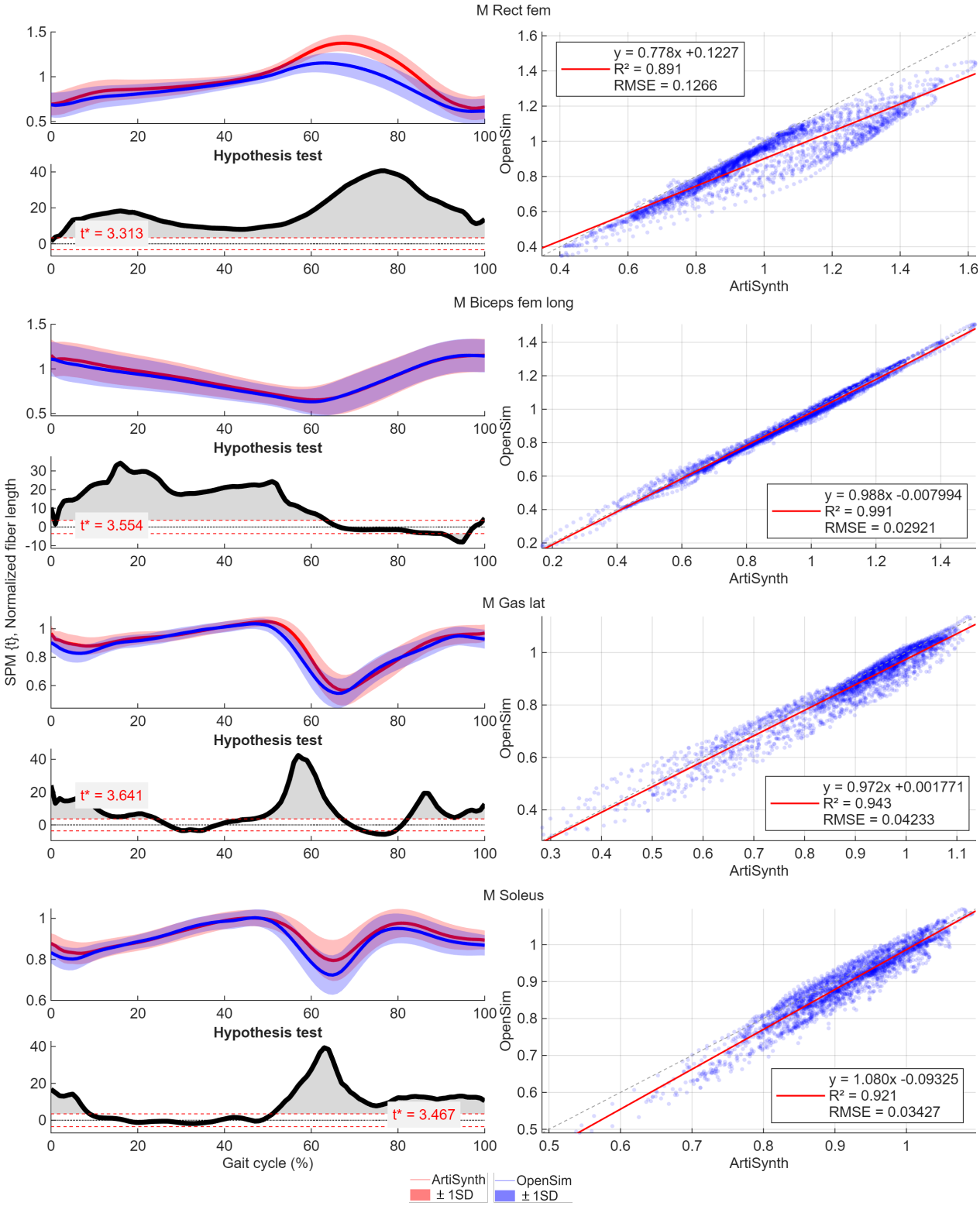


Figure 6. Computed normalized fiber lengths SPM (**left**) and RMS (**right**) during FD from OpenSim computations (blue) and ArtiSynth computations (red). Each curve represents the average of 28 representative trials ± one standard deviation. All tests were performed with $\alpha = 0.05$ on 28 representative trials. Suprathresholds are indicated by t^* for every test. RMS were fitted linearly; identity is indicated as gray dashed line.

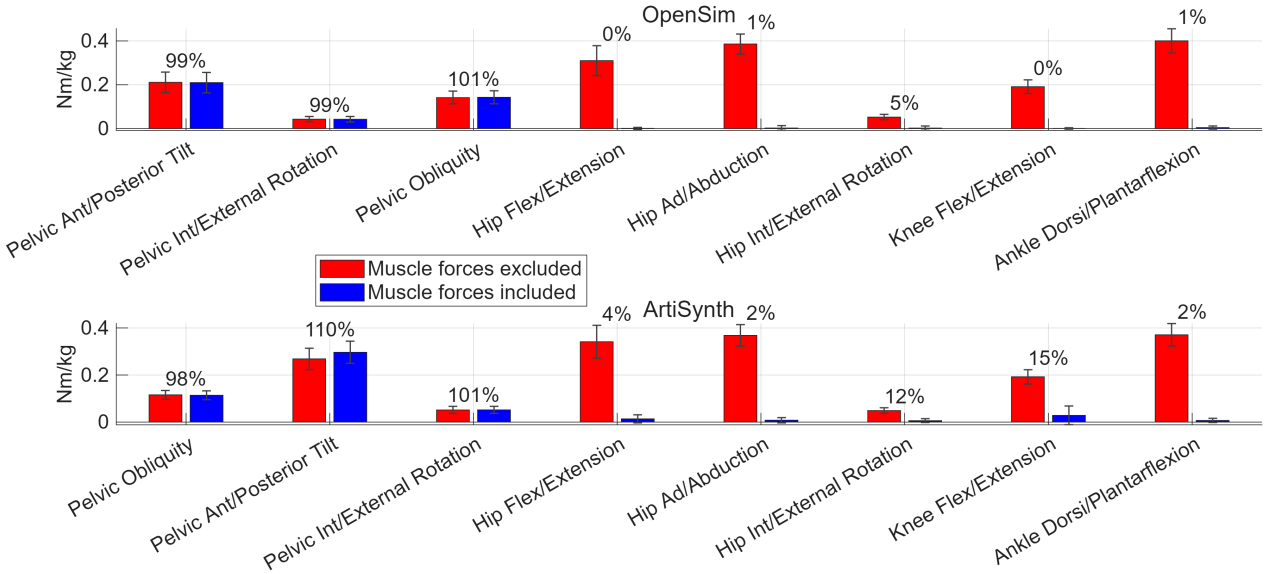


Figure 7. Absolute mean joint moment (± one standard deviation) from 28 representative trials that was generated by reserve actuators during forward dynamics in OpenSim (**top**) and ArtiSynth (**bottom**). Simulations with excluded muscle forces are shown in red vs. simulations including muscle forces shown in blue. Ratios (%) indicate the amount of joint moment that was generated when muscle forces were included with respect to the net joint moment for better comparability.

4. Discussion

This work set out to establish a functioning ArtiSynth model of the lower limb that ensures plausible reproduction of physiologically reasonable kinematics and kinetics during gait for a broad range of healthy participants. We compared ArtiSynth outputs to OpenSim (IK, joint moments, muscle forces and reserve actuator recruitment) to prepare the groundwork for future combined MB-FE studies. The resulting model provides all settings and interfaces that users expect from OpenSim, namely, properties for joints, muscles, and the inverse controller, making future comparisons straightforward.

It turned out that ArtiSynth, as is, did not reproduce the same model output across all investigated trials, partly because 10 % of the evaluated trials did not pass criterion 1. Five out of those nine trials already failed at the Inverse Kinematics stage, and of the remaining 4, solving via fallback was not identified as driving force behind not meeting criterion 1. However, it must be noted that the tracking RMS error from ArtiSynth forward dynamics simulations with muscles included is arguably the highest. This study has no independent validation cohort but used a subset of the available trials for calibration. However, we did not observe the simulations to be overly fitted to the calibration set. Therefore, using a bilevel optimization setup to identify optimal marker tracking weights on a calibration trial set was an appropriate approach in this study. The reserve actuator recruitment screening revealed that simulation stability primarily depends on balancing regularization to excitation damping, and we recommend to reset $w_{m,a,d}$ when entering fallback mode instead of tuning those to a value that is suitable for both modes. In the worst case, all aforementioned parameters might need subject specific tuning. Nevertheless, we also observed that trials tend to recover well from a small amount of solves in fallback mode, such that we deem the selected parameters sufficient in this study.

Across participants, ArtiSynth and OpenSim produced nearly identical results in terms of computed joint angles, even though all joint angles differed significantly. Given the results of earlier comparative studies, this is to be expected [39–42]. However, all reported joint angle differences in this study fall below or in the same range of other studies using the RMS as the error metric between frameworks [41]. The computed joint angles are consistent

with the literature using the PiG markerset or other OpenSim gait models [40,72,73,78]. Schwartz et al. developed a repository of comprehensive gait data for a large group of children [73], and Bovi et al. published a multi-task gait analysis protocol applied to 40 individuals [72]. This data pool was later extended by Monteiro et al [24]. Roelker et al. performed a computational study to test for the differences between four OpenSim gait models of varying complexity that produced similar results [40]. When comparing our results to experimental data, one must note that Vicon uses virtual joint centers to compute joint angles [48], where differences might arise.

The confidence intervals provide additional context for interpreting the statistically significant waveform differences. Despite widespread differences identified by SPM, the RMSE confidence intervals remained entirely below the predefined kinematic agreement threshold during IK and muscle-excluded FD. This supports the interpretation that statistically significant waveform differences do not necessarily imply biomechanically substantial discrepancies. However, muscle-driven FD showed less consistent agreement. In particular, the knee flexion RMSE exceeded the threshold entirely, while hip flexion and ankle dorsiflexion remained inconclusive. These findings suggest that kinematic reproducibility is less robust when the trajectories are generated through muscle-driven simulations rather than idealized joint actuation.

Computed joint moments agree well in overall shape and magnitude, but statistically significant differences were found in all joints. It should be noted that our joint moment RMS errors exceed the errors of similar studies, although the underlying joint moments are in the same range [41]. Our computed joint moments are in line with other published kinetic data [24,40,72,73,79]. However, since joint moments are inherently affected by the coordinate system origin of the respective joint, a direct comparison, especially to data from motion capturing systems, is oftentimes misleading. The studies by Monteiro et al, Bovi et al., and Schwartz et al. were experimental [24,72,73], while Roelker et al., and Rajagopal et al. did computations [40,79], yet all findings correspond well with our results in shape and magnitude. Bergmann et al. studied load transmission patterns in instrumented knee implants for various activities [80]. There are several limitations to the comparability; the evaluated patients were all above age 62 and consisted of average and high body weight individuals, with the knee joint coordinate system located on the tibial plateau. However, they reported (absolute) knee joint flexion moments ranging between 0 and 20 Nm. They correspond well in general shape and also in magnitude, given the average patient weight of 72.6 kg in our study.

The most notable difference is that ArtiSynth simulations produced pelvis joint moments with greater transients and larger absolute values. This could be explained by several reasons. First and foremost, both solvers relied on different cost functions, so solutions may have converged to different excitation patterns, even if both actuator sets were identical. OpenSim's CMC algorithm tracks joint coordinates from IK, whereas ArtiSynth tracks marker positions. Therefore, ArtiSynth uses the "default" marker weights also used for IK, while tracking weights for joint angles need to be set explicitly in OpenSim. The latter were set to counteract pelvis drop specifically for better tracking (Table S4). This is especially crucial if RRA is not part of the simulation pipeline. The GRF values are zero at $t = 0$, which is physically equivalent to being in free fall, while the prescribed joint/marker kinematics drive the model forward—the residual is then distributed differently across the available DoF in both frameworks and fades after the GRF provide counteracting forces and moments. Since ArtiSynth does not provide a functionality similar to RRA, we recommend to treat the computed joint moments during the first time steps as the initialization phase, similar to the offset of 0.03 s OpenSim describes when interpreting CMC results [58]. Also, we used pre-simulation velocity filtering via Savitzky–Golay filtering, whereas OpenSim lowpasses

their trajectories and kinematic data prior to computation using a butterworth filter, possibly leading to subtle numerical differences for particular values.

The kinetic guidelines defined by [65] were violated in almost all time steps and simulations. The authors constructed a bilevel optimization scheme to minimize the residuals during RRA until meeting all aforementioned criteria. Interestingly, the authors found that guidelines 3a and 3c were almost always met in their simulations, while in this study, guideline 3c was the one being violated most often. A way to reduce the violations of the kinetic guidelines would be to adapt RRA into the ArtiSynth pipeline and possibly to incorporate the kinetic guidelines themselves into an outer optimization routine.

Both frameworks diverged extensively in terms of computed muscle forces; statistically significant differences were found for every investigated muscle. Refs. [24,72,73] provide EMG data. It should be noted that EMG data do not directly validate muscle force magnitude, but in terms of shape and timing, our computed muscle forces are in line with experimental BF, GM, and SOL data, and they also correspond partly to the computed muscle forces in OpenSim. RF and VM muscles, however, do not correspond to experimental EMG data, and notably, these and SM are the muscles with the most discrepancy to OpenSim simulations as well. The current muscle forces may not be interpreted as physiologically reasonable unless experimental verification of the forces is provided. On the other hand, normalized fiber lengths mostly agreed closely, corresponding to matching model poses throughout the gait cycle and also to the normalized fiber lengths reported by [81]; they computed normalized fiber lengths for walking and running at different speeds. However, there are distinct differences in the RF and VM muscles between 60 and 80% of the gait cycle. There might be several reasons for that. Most importantly, ArtiSynth does not simulate muscle activation dynamics. A computed excitation directly translates to the corresponding muscle activation without delay; therefore, excitation damping was added to the cost term of Equation (15), although OpenSim does not feature such a term. While excitation damping certainly does prevent rapid excitation changes, first, it does so on a global scale and thereby also damps reserve actuator excitations. Secondly, excitation damping acts symmetrically on rising and falling excitation changes, whereas default activation dynamics feature different constants to model the response to rising and falling edges individually. The default muscle model of OpenSim is based on works by Thelen [82] and uses 10 ms and 40 ms for activation and deactivation, respectively [83]. So, the muscles take four times as long to deactivate as to activate, whereas in ArtiSynth, muscle excitations can decrease more rapidly if not demanded. In scenarios of rapidly changing boundary conditions, ArtiSynth muscle models might be more likely to jitter. A possible solution could be to extend the inverse solving capabilities of ArtiSynth to also prescribe excitation targets. This would enable to provide EMG data on certain muscles, leading to EMG-informed muscle control. On the OpenSim side, there are already tools for that like OpenSim-Moco or CEINMS [84,85].

Reserve actuators were recruited quite similarly across hip flexion, rotation and ankle dorsiflexion. In those joints, reserve actuators contributed less than 5 % of the net joint moment. However, this threshold also was exceeded by the hip rotation and knee flexion reserve actuators. Great correspondence was observed in those actuators supporting the pelvis only. Since the latter provide the residuals needed to stabilize the model in space, this corresponds to similar violation patterns of criterion 3. The observed transient behavior at the beginning of the gait cycle still persists when muscles are added to the model. Greater muscle effort and/or less reserve actuator recruitment is achieved by increasing the reserve-actuator-to-muscle-weight ratio. A way to reduce current recruitment could be to bound the JA excitations in ArtiSynth in the interval $[-1000, 1000]$ while simultaneously decreasing their maximum force. This would introduce a new axis of excitation cost to the controller—however, the interplay with the excitation damping term needs further inves-

tigation then, since increasing the excitations also increases the corresponding excitation changes between time steps. In the current configuration, the results probably indicate that JA recruitment in hip rotation and knee flexion was not penalized appropriately and not that the muscles were insufficient to generate the required torques.

These outcomes underline the sensitivity of both solvers to the objective and cost functions, numerical settings, and muscle-tendon parameterization, and therefore, this study can only serve to compare complete computational pipelines rather than isolating the influence of the software platforms alone. All the aforementioned parameters have been subject to sensitivity and/or calibration studies in the past. Although a minimized squared activation is common as a surrogate for metabolic cost, various frameworks suggest extended or more complex cost functions [21,86–88]. Likewise, numerous studies have shown strong sensitivity to Hill-type parameters, especially optimal fiber length, tendon slack length, and maximum isometric force [89–96] or to conceptual differences, such as tendon compliance assumptions (rigid vs. compliant) [68,97]. Moreover, all aforementioned parameters were derived from cadaveric studies with debatable suitability for accurate muscle dynamics reproduction [98].

There are several additional limitations to this study apart from those already mentioned; first and foremost, this comparison was based on a specific participant group, including only healthy adults. The findings cannot be generalized to pathological gait, younger athletic populations, running, stair negotiation, shoed walking or other demanding activities. Also, this study used one gait cycle per trial, which was supported by force plate contact. There are numerous studies that evaluated methods to predict ground reaction forces [99] and moments [100,101] from kinematic data with varying accuracy. Using these could unlock more trials per participant, thereby providing the SMaRT algorithm with a broader set of trials to choose from. Selecting representative trials based on the OpenSim dataset made the benchmark asymmetric, possibly favoring the reference pipeline. It is suggested to select representative trials from experimental data before any simulation takes place in the future. Since no correction was applied to the results of the SPM paired tests, the results of this study are only exploratory. Also, our results are limited by the quality of the scaling procedure. The effect of different scaling techniques and weights on kinematic and kinetic results is an ongoing topic [69,102,103]. A more subject-specific scaling technique for participants diverging from "norm" geometries could enhance the respective predictions and is worth studying further. Moreover, the presented model relies on a PiG-based OpenSim model rather than on more advanced models, like [79]. However, prior assessments from [40] suggest that the current model complexity is often sufficient for basic gait patterns of healthy participants. Additionally, the assigned total weight of 1.6×10^{-4} kg to scapulae and clavicles might have affected the whole-body dynamics.

In summary, this study successfully established a multibody model in ArtiSynth. Our data support strong kinematic reproducibility, but only partial kinetic agreement and substantial differences in muscle recruitment. Given that reserve contribution scaled with the weightings in the objective function, we believe that differences in recruited muscle and reserve actuator forces reflect the different optimization approaches rather than poor framework performance in itself. However, in the current configuration, the observed differences are not acceptable for the intended future use, since muscle/reserve actuator forces act as boundary conditions and likely propagate to the tissue level and require continuous improvement. Specifically, reserve actuator contribution in hip and knee flexion, as well as the kinetic guideline violations, need to be addressed. Also, this model requires independent validation. As this model aims to serve as a foundation for future combined MB-FE simulations, it is crucial to understand how differences in activation and muscle-tendon properties will propagate to tissue-level predictions. We plan to investigate these

issues in a broader calibration study in the future in a combined model including soft tissues. Although this model provides kinematically reasonable results, it may not yet be suitable as a foundation for non-invasive analyses of the mechanics of biological systems.

Supplementary Materials: The following supporting information can be downloaded at: https://www.mdpi.com/article/10.3390/biomechanics6040110/s1, Table S1: Marker tracking error after evaluating IK results of the static trial used for scaling. Baseline was done with all group weights set to 1. The coordinate tasks were defined with a weight of 1 for the ankle, subtalar and metatarsophalangeal angles; Table S2: Group names and included markers per group.; Table S3: Assigned group weights during inverse kinematics computations; Figure S1: Histogram showing the IK marker tracking error distribution in the calibration set (blue) and all trials (blue + grey). Mean tracking error is 12.88 mm for the calibration set and 13.36 mm for all trials. Note, that four trials exceed the acceptable threshold of 20 mm defined by [7]; Table S4: Assigned task set weights during force set replacement (W_{rep}) and extension (W_{ext}), and corresponding reserve actuator optimal forces (F^{opt}_{rep}, F^{opt}_{ext}). Not assigned tasks are indicated by "-". Since the model does not feature any muscles in the upper body, the corresponding joints were assigned the same optimal force. Weights and optimal forces were assigned symmetrically; Figure S2: Heatmaps of the pooled first screening results across all 10 trials. Mean percentage of time steps/number of trials with more than 50% of time steps solved using equality constraints (top left). Mean tracking RMS error (top right). Mean joint moment generated by the JAs (bottom left) and combined muscle effort (bottom right). The final parameter set is outlined in black, trading-off mean JA recruitment and muscle effort against more accurate tracking and stable solving; Figure S3: Heatmap of the pooled second screening results across all 10 trials. Mean percentage of time steps/number of trials with more than 50% of time steps solved using equality constraints (top left). Mean tracking RMS error (top right). Mean joint moment generated by JAs (bottom left) abd combined muscle effort (bottom right). The final parameter set is outlined in black; Table S5: Simulation results of all available 90 evaluation-set trials before passing them to SMaRT. Number of calibration-set trials not meeting criterion 1 (first column) are provided in brackets behind the number of evaluation-set trials; Figure S4: Tracking RMS error added to the Inverse Kinematics tracking error against the percentage of time steps solved in fallback mode, shown for the 31 of 90 trials entering fallback. Trials whose Inverse Kinematics tracking error already missed criterion 1 are outlined; Figure S5: Detailed results of the SPM tests on joint angles from IK. All tests were performed with $\alpha = 0.05$ on 28 representative trials. Suprathresholds are indicated by t^* for every test; Figure S6: Detailed results of the joint angle RMS errors from IK including 28 representative trials. RMS was fitted with a linear regression model, identity is depicted as grey dashed line; Figure S7: Detailed results of the SPM tests on joint angles from FD with muscles excluded. All tests were performed with $\alpha = 0.05$ on 28 representative trials. Suprathresholds are indicated by t^* for every test; Figure S8: Detailed results of the joint angle RMS errors from FD with muscles excluded, including 28 representative trials. RMS was fitted with a linear regression model, identity is depicted as grey dashed line; Figure S9: Detailed results of the SPM tests on joint angles from FD with muscles included. All tests were performed with $\alpha = 0.05$ on 28 representative trials. Suprathresholds are indicated by t^* for every test; Figure S10: Detailed results of the joint angle RMS errors from FD with muscles included, including 28 representative trials. RMS was fitted with a linear regression model, identity is depicted as grey dashed line; Figure S11: Detailed results of the SPM tests on joint moments from FD with muscle excluded. All tests were performed with $\alpha = 0.05$ on 28 representative trials. Suprathresholds are indicated by t^* for every test; Figure S12: Detailed results of the joint moment RMS errors from FD with muscle excluded, including 28 representative trials. RMS was fitted with a linear regression model, identity is depicted as grey dashed line; Figure S13: Guideline violation plot for one exemplary representative trial, adapted from the MATLAB tool provided by [11]. FD with excluded muscle forces is shown for ArtiSynth (top) and OpenSim (bottom). The transient phase is especially visible in the ZMP trajectory; Figure S14: Detailed results of the SPM tests on muscle forces from FD with muscle forces included. All tests were performed with $\alpha = 0.05$ on 28 representative trials. Suprathresholds are indicated by t^* for every test; Figure S15: Detailed results of the muscle force RMS errors from FD with muscle forces included, including 28 representative trials. RMS was fitted with a linear regression model, identity is depicted as grey dashed line; Figure S16: Detailed results of the SPM tests on normalized fiber lengths from FD with muscle forces included.

All tests were performed with $\alpha = 0.05$ on 28 representative trials. Suprathresholds are indicated by t^* for every test; Figure S17: Detailed results of the normalized muscle fiber length RMS errors from FD with muscle forces included, including 28 representative trials. RMS was fitted with a linear regression model, identity is depicted as grey dashed line; Figure S18: Detailed results of the SPM tests on reserve actuator recruitment during FD with muscle forces included. All tests were performed with $\alpha = 0.05$ on 28 representative trials. Suprathresholds are indicated by t^* for every test; Figure S19: Detailed results of the reserve actuator recruitment RMS errors during FD with muscle forces included, including 28 representative trials. RMS was fitted with a linear regression model, identity is depicted as grey dashed line.

Author Contributions: Conceptualization, A.G.; methodology, A.G.; software, A.G.; validation, A.G.; formal analysis, A.G.; investigation, A.G.; writing—original draft preparation, A.G.; writing—review and editing, A.G. and W.K.; visualization, A.G.; supervision, W.K.; funding acquisition, W.K. All authors have read and agreed to the published version of the manuscript.

Funding: This research received no external funding.

Institutional Review Board Statement: The study was conducted in accordance with the Declaration of Helsinki and approved by Ethics Committee of the University Duisburg-Essen (application number 18.7988).

Informed Consent Statement: Informed consent was obtained from all subjects involved in the study.

Data Availability Statement: The data presented in this study are available upon request from the corresponding author due to privacy reasons.

Acknowledgments: The authors would like to acknowledge John E. Lloyd (University of British Columbia, Vancouver) for his continued and invaluable technical assistance and support throughout this study. Also, the authors wish to acknowledge Francisco Geu Flores (University of Duisburg-Essen, Duisburg) and Dominik Raab (University of Duisburg-Essen, Duisburg) for their thorough professional feedback throughout the study.

Conflicts of Interest: The authors declare no conflicts of interest.

Abbreviations

The following abbreviations are used in this manuscript:

MB	multibody
FE	finite element
PiG	Plug-in Gait
IK	inverse kinematics
FD	forward dynamics
RRA	residual reduction algorithm
ID	inverse dynamics
GRF	ground reaction forces
GRM	ground reaction moments
CMC	computed muscle control
CoP	center of pressure
JA	joint actuator
RF	rectus femoris
BF	biceps femoris
GL	gastrocnemius lateralis
GM	gastrocnemius medialis
VM	vastus medialis
SM	semimembranosus
SOL	soleus
SMaRT	selection method for a representative trial
PCA	principal component analysis
SPM	statistical parametric mapping
RMS	root mean square error

References

1. Innocenti, B.; Bori, E.; Armaroli, F.; Schlager, B.; Jonas, R.; Wilke, H.J.; Galbusera, F. The use of computational models in orthopedic biomechanical research. In *Human Orthopaedic Biomechanics*; Innocenti, B., Galbusera, F., Eds.; Elsevier: Amsterdam, The Netherlands, 2022; pp. 681–712. [CrossRef]
2. Xu, D.; Zhou, H.; Wang, M.; Ma, X.; Gusztav, F.; Chon, T.E.; Fernandez, J.; Baker, J.S.; Gu, Y. Contribution of ankle motion pattern during landing to reduce the knee-related injury risk. *Comput. Biol. Med.* **2024**, *180*, 108965. [CrossRef]
3. Sabatini, A.L.; Goswami, T. Hip implants VII: Finite element analysis and optimization of cross-sections. *Mater. Des.* **2008**, *29*, 1438–1446. [CrossRef]
4. Ceddia, M.; Solarino, G.; Cassano, G.D.; Trentadue, B. Finite Element Study on Stability in the Femoral Neck and Head Connection to Varying Geometric Parameters with the Relates Implications on the Effect of Wear. *J. Compos. Sci.* **2023**, *7*, 387. [CrossRef]
5. Galbusera, F.; Freutel, M.; Dürselen, L.; D'Aiuto, M.; Croce, D.; Villa, T.; Sansone, V.; Innocenti, B. Material models and properties in the finite element analysis of knee ligaments: A literature review. *Front. Bioeng. Biotechnol.* **2014**, *2*, 54. [CrossRef]
6. Menzel, A.; Kuhl, E. Frontiers in growth and remodeling. *Mech. Res. Commun.* **2012**, *42*, 1–14. [CrossRef]
7. Phillips, A.T.; Villette, C.C.; Modenese, L. Femoral bone mesoscale structural architecture prediction using musculoskeletal and finite element modelling. *Int. Biomech.* **2015**, *2*, 43–61. [CrossRef]
8. Liukkonen, M.K.; Mononen, M.E.; Klets, O.; Arokoski, J.P.; Saarakkala, S.; Korhonen, R.K. Simulation of Subject-Specific Progression of Knee Osteoarthritis and Comparison to Experimental Follow-up Data: Data from the Osteoarthritis Initiative. *Sci. Rep.* **2017**, *7*, 9177. [CrossRef]
9. Hosseini, S.M.; Wilson, W.; Ito, K.; van Donkelaar, C. A numerical model to study mechanically induced initiation and progression of damage in articular cartilage. *Osteoarthr. Cartil.* **2014**, *22*, 95–103. [CrossRef]
10. Waffenschmidt, T. Modelling and Simulation of Adaptation and Degradation in Anisotropic Biological Tissues. Ph.D. Thesis, Technische Universität Dortmund, Dortmund, Germany, 2013.
11. Nispel, K.; Lerchl, T.; Senner, V.; Kirschke, J.S. Recent Advances in Coupled MBS and FEM Models of the Spine—A Review. *Bioengineering* **2023**, *10*, 315. [CrossRef]
12. Stops, A.; Wilcox, R.; Jin, Z. Computational modelling of the natural hip: A review of finite element multibody simulations. *Comput. Methods Biomech. Biomed. Eng.* **2013**, *15*, 963–979. [CrossRef]
13. Remus, R.; Selkmann, S.; Lipphaus, A.; Neumann, M.; Bender, B. Muscle-driven forward dynamic active hybrid model of the lumbosacral spine: Combined FEM and multibody simulation. *Front. Bioeng. Biotechnol.* **2023**, *11*, 1223007. [CrossRef]
14. Carpenedo, L.; Ignasiak, D.; Remus, R.; La Barbera, L. Advances in Musculoskeletal Modeling of the Thoraco-Lumbar Spine: A Comprehensive Systematic Review. *Ann. Biomed. Eng.* **2025**, *53*, 2883–2910. [CrossRef]
15. Esrafilian, A.; Stenroth, L.; Mononen, M.E.; Tanska, P.; van Rossom, S.; Lloyd, D.G.; Jonkers, I.; Korhonen, R.K. 12 Degrees of Freedom Muscle Force Driven Fibril-Reinforced Poroviscoelastic Finite Element Model of the Knee Joint. *IEEE Trans. Neural Syst. Rehabil. Eng. Publ. IEEE Eng. Med. Biol. Soc.* **2021**, *29*, 123–133. [CrossRef]
16. Luboz, V.; Perrier, A.; Stavness, I.; Lloyd, J.E.; Bucki, M.; Cannard, F.; Diot, B.; Vuillerme, N.; Payan, Y. Foot ulcer prevention using biomechanical modelling. *Comput. Methods Biomech. Biomed. Eng.* **2012**, *2*, 189–196. [CrossRef]
17. Esrafilian, A.; Stenroth, L.; Mononen, M.E.; Tanska, P.; Avela, J.; Korhonen, R.K. EMG-Assisted Muscle Force Driven Finite Element Model of the Knee Joint with Fibril-Reinforced Poroelastic Cartilages and Menisci. *Sci. Rep.* **2020**, *10*, 3026. [CrossRef]
18. Park, S.; Lee, S.; Yoon, J.; Chae, S.W. Finite element analysis of knee and ankle joint during gait based on motion analysis. *Med. Eng. Phys.* **2019**, *63*, 33–41. [CrossRef]
19. Halonen, K.S.; Dzialo, C.M.; Mannisi, M.; Venäläinen, M.S.; de Zee, M.; Andersen, M.S. Workflow assessing the effect of gait alterations on stresses in the medial tibial cartilage - combined musculoskeletal modelling and finite element analysis. *Sci. Rep.* **2017**, *7*, 17396. [CrossRef]
20. Marouane, H.; Shirazi-Adl, A.; Adouni, M. 3D active-passive response of human knee joint in gait is markedly altered when simulated as a planar 2D joint. *Biomech. Model. Mechanobiol.* **2017**, *16*, 693–703. [CrossRef]
21. Navacchia, A.; Hume, D.R.; Rullkoetter, P.J.; Shelburne, K.B. A computationally efficient strategy to estimate muscle forces in a finite element musculoskeletal model of the lower limb. *J. Biomech.* **2019**, *84*, 94–102. [CrossRef]
22. Ali, A.A.; Shalhoub, S.S.; Cyr, A.J.; Fitzpatrick, C.K.; Maletsky, L.P.; Rullkoetter, P.J.; Shelburne, K.B. Validation of predicted patellofemoral mechanics in a finite element model of the healthy and cruciate-deficient knee. *J. Biomech.* **2016**, *49*, 302–309. [CrossRef]
23. Lenhart, R.L.; Kaiser, J.; Smith, C.R.; Thelen, D.G. Prediction and Validation of Load-Dependent Behavior of the Tibiofemoral and Patellofemoral Joints During Movement. *Ann. Biomed. Eng.* **2015**, *43*, 2675–2685. [CrossRef]
24. Monteiro, N.M.B.; Da Silva, M.P.T.; Folgado, J.O.M.G.; Melancia, J.P.L. Structural analysis of the intervertebral discs adjacent to an interbody fusion using multibody dynamics and finite element cosimulation. *Multibody Syst. Dyn.* **2011**, *25*, 245–270. [CrossRef]
25. Hume, D.R.; Rullkoetter, P.J.; Shelburne, K.B. ReadySim: A computational framework for building explicit finite element musculoskeletal simulations directly from motion laboratory data. *Int. J. Numer. Methods Biomed. Eng.* **2020**, *36*, e3396. [CrossRef]

26. Lloyd, J.E.; Stavness, I.; Fels, S. Artisynth: A Fast Interactive Biomechanical Modeling Toolkit Combining Multibody and Finite Element Simulation. In *Soft Tissue Biomechanical Modeling for Computer Assisted Surgery*; Payan, Y., Ed.; Springer: Berlin/Heidelberg, Germany, 2012; pp. 355–394.
27. Wu, X.; Sánchez, C.A.; Lloyd, J.E.; Borgard, H.; Fels, S.; Paydarfar, J.A.; Halter, R.J. Estimating tongue deformation during laryngoscopy using a hybrid FEM-multibody model and intraoperative tracking—A cadaver study. *Comput. Methods Biomech. Biomed. Eng.* **2025**, *28*, 739–749. [CrossRef]
28. Elyasi, E.; Perrier, A.; Bailet, M.; Payan, Y. Biomechanical lower limb model to predict patellar position alteration after medial open wedge high tibial osteotomy. *J. Biomech.* **2022**, *136*, 111062. [CrossRef]
29. Malakoutian, M.; Sanchez, C.A.; Brown, S.H.M.; Street, J.; Fels, S.; Oxland, T.R. Biomechanical Properties of Paraspinal Muscles Influence Spinal Loading-A Musculoskeletal Simulation Study. *Front. Bioeng. Biotechnol.* **2022**, *10*, 852201. [CrossRef]
30. Remus, R.; Lipphaus, A.; Neumann, M.; Bender, B. Calibration and validation of a novel hybrid model of the lumbosacral spine in ArtiSynth—The passive structures. *PLoS ONE* **2021**, *16*, e0250456. [CrossRef]
31. Sagl, B.; Schmid-Schwap, M.; Piehslinger, E.; Kundi, M.; Stavness, I. A Dynamic Jaw Model With a Finite-Element Temporomandibular Joint. *Front. Physiol.* **2019**, *10*, 1156. [CrossRef]
32. Stavness, I.; Lloyd, J.E.; Fels, S. Automatic prediction of tongue muscle activations using a finite element model. *J. Biomech.* **2012**, *45*, 2841–2848. [CrossRef]
33. Stavness, I.; Lloyd, J.E.; Payan, Y.; Fels, S. Coupled hard-soft tissue simulation with contact and constraints applied to jaw-tongue-hyoid dynamics. *Int. J. Numer. Methods Biomed. Eng.* **2011**, *27*, 367–390. [CrossRef]
34. Delp, S.L.; Anderson, F.C.; Arnold, A.S.; Loan, P.; Habib, A.; John, C.T.; Guendelman, E.; Thelen, D.G. OpenSim: Open-source software to create and analyze dynamic simulations of movement. *IEEE Trans. Bio-Med. Eng.* **2007**, *54*, 1940–1950. [CrossRef]
35. v. Kistowski, J.; Arnold, J.A.; Huppler, K.; Lange, K.D.; Henning, J.L.; Cao, P. How to Build a Benchmark. In Proceedings of the ICPE '15: Proceedings of the 6th ACM/SPEC International Conference on Performance Engineering, ICPE '15, New York, NY, USA, 31 January–4 February 2015; pp. 333–336. [CrossRef]
36. Masoudi, R.; Uchida, T.; Vilela, D.; Luaces, A.; Cuadrado, J.; McPhee, J. A library of computational benchmark problems for the multibody dynamics community. In Proceedings of the ECCOMAS Thematic Conference on Multibody Dynamics 2013, Zagreb, Croatia, 1–4 July 2013; pp. 1153–1162.
37. Bauchau, O.A.; Betsch, P.; Cardona, A.; Gerstmayr, J.; Jonker, B.; Masarati, P.; Sonneville, V. Validation of flexible multibody dynamics beam formulations using benchmark problems. *Multibody Syst. Dyn.* **2016**, *37*, 29–48. [CrossRef]
38. Gonçalves, S.B.; Rodrigues da Silva, M.; Marques, F.; Flores, P.; Tavares da Silva, M. Validation of skeletal muscle models in multibody dynamics: A collaborative collection of benchmark cases. *Multibody Syst. Dyn.* **2026**, *66*, 1057–1100. [CrossRef]
39. Wagner, D.W.; Stepanyan, V.; Shippen, J.M.; DeMers, M.S.; Gibbons, R.S.; Andrews, B.J.; Creasey, G.H.; Beaupre, G.S. Consistency among musculoskeletal models: Caveat utilitor. *Ann. Biomed. Eng.* **2013**, *41*, 1787–1799. [CrossRef]
40. Roelker, S.A.; Caruthers, E.J.; Baker, R.K.; Pelz, N.C.; Chaudhari, A.M.W.; Siston, R.A. Interpreting Musculoskeletal Models and Dynamic Simulations: Causes and Effects of Differences Between Models. *Ann. Biomed. Eng.* **2017**, *45*, 2635–2647. [CrossRef]
41. Falisse, A.; van Rossom, S.; Gijsbers, J.; Steenbrink, F.; van Basten, B.J.H.; Jonkers, I.; van den Bogert, A.J.; de Groote, F. OpenSim Versus Human Body Model: A Comparison Study for the Lower Limbs During Gait. *J. Appl. Biomech.* **2018**, *34*, 496–502. [CrossRef]
42. Trinler, U.; Schwameder, H.; Baker, R.; Alexander, N. Muscle force estimation in clinical gait analysis using AnyBody and OpenSim. *J. Biomech.* **2019**, *86*, 55–63. [CrossRef]
43. Jäger, M.; Mayer, C.; Hefter, H.; Siebler, M.; Kecskeméthy, A. Big Data und maschinelles Lernen bei Prävention und Rehabilitation. *Die Orthop.* **2018**, *47*, 826–833. [CrossRef]
44. Kecskeméthy, A.; Siebler, M.; Raab, D.; Geu Flores, F.; Hefter, H. ReHabX: Personalisierte Therapiesteuerung bei Gangstörungen am Beispiel des Schlaganfalls. In *Digitale Transformation von Dienstleistungen im Gesundheitswesen V*; Pfannstiel, M.A., Da-Cruz, P., Mehlich, H., Eds.; Springer Fachmedien Wiesbaden: Wiesbaden, Austria, 2019; pp. 237–254.
45. Pinto Ferreira, P.D. Development of Functional Numerical Scores for Improving the Diagnostic of Motion Impairment of Stroke Patients Using Non-Traditional Gait Parameters. Doctoral's Dissertation, Universität Duisburg-Essen, Duisburg, Germany, 2016.
46. Dorn, T. Plug In Gait Model & Markerset. Available online: https://simtk.org/frs/?group_id=433. (accessed on 12 August 2026).
47. Hamner, S.R.; Seth, A.; Delp, S.L. Muscle contributions to propulsion and support during running. *J. Biomech.* **2010**, *43*, 2709–2716. [CrossRef]
48. Vicon Motion Systems Ltd. Vicon Plug-in Gait Reference Guide. Available online: https://help.vicon.com/download/attachments/11378719/Plug-in%20Gait%20Reference%20Guide.pdf (accessed on 12 August 2026).
49. Leardini, A.; Caravaggi, P.; Theologis, T.; Stebbins, J. Multi-segment foot models and their use in clinical populations. *Gait Posture* **2019**, *69*, 50–59. [CrossRef]

50. Veerkamp, K.; van der Krogt, M.M.; Waterval, N.F.J.; Geijtenbeek, T.; Walsh, H.P.J.; Harlaar, J.; Buizer, A.I.; Lloyd, D.G.; Carty, C.P. Predictive simulations identify potential neuromuscular contributors to idiopathic toe walking. *Clin. Biomech.* **2024**, *111*, 106152. [CrossRef]
51. OpenSim. Scaling. 2018. Available online: https://opensimconfluence.atlassian.net/wiki/spaces/OpenSim/pages/53090000/Scaling (accessed on 12 August 2026).
52. Werling, K.; Bianco, N.A.; Raitor, M.; Stingel, J.; Hicks, J.L.; Collins, S.H.; Delp, S.L.; Liu, C.K. AddBiomechanics: Automating model scaling, inverse kinematics, and inverse dynamics from human motion data through sequential optimization. *bioRxiv* **2023**. [CrossRef]
53. Reinbolt, J.A.; Schutte, J.F.; Fregly, B.J.; Koh, B.I.; Haftka, R.T.; George, A.D.; Mitchell, K.H. Determination of patient-specific multi-joint kinematic models through two-level optimization. *J. Biomech.* **2005**, *38*, 621–626. [CrossRef]
54. Barré, A.; Jolles, B.M.; Theumann, N.; Aminian, K. Soft tissue artifact distribution on lower limbs during treadmill gait: Influence of skin markers' location on cluster design. *J. Biomech.* **2015**, *48*, 1965–1971. [CrossRef]
55. Bakke, D.; Besier, T. Shape-model scaled gait models can neglect segment markers without consequential change to inverse kinematics results. *J. Biomech.* **2022**, *137*, 111086. [CrossRef]
56. OpenSim. Residual Reduction Algorithm. 2018. Available online: https://opensimconfluence.atlassian.net/wiki/spaces/OpenSim/pages/53089669/Residual+Reduction+Algorithm (accessed on 12 August 2026).
57. Thelen, D.G.; Anderson, F.C. Using computed muscle control to generate forward dynamic simulations of human walking from experimental data. *J. Biomech.* **2006**, *39*, 1107–1115. [CrossRef]
58. OpenSim. Computed Muscle Control. 2018. Available online: https://opensimconfluence.atlassian.net/wiki/spaces/OpenSim/pages/53089719/Computed+Muscle+Control (accessed on 12 August 2026).
59. OpenSim. Analyses. 2018. Available online: https://opensimconfluence.atlassian.net/wiki/spaces/OpenSim/pages/53089589/Analyses (accessed on 12 August 2026).
60. ArtiSynth Modeling Guide. Chapter 10 Inverse Simulation. Available online: https://www.artisynth.org/manuals/index.jsp (accessed on 1 October 2025).
61. Crenna, F.; Rossi, G.B.; Berardengo, M. Filtering Biomechanical Signals in Movement Analysis. *Sensors* **2021**, *21*, 4580. [CrossRef]
62. Schafer, R. What Is a Savitzky-Golay Filter? *IEEE Signal Process. Mag.* **2011**, *28*, 111–117. [CrossRef]
63. Uchida, T.K.; Delp, S.L. *Biomechanics of Movement: The Science of Sports, Robotics, and Rehabilitation*; The MIT Press: Cambridge, MA, USA, 2020.
64. Hicks, J.L.; Uchida, T.K.; Seth, A.; Rajagopal, A.; Delp, S.L. Is my model good enough? Best practices for verification and validation of musculoskeletal models and simulations of movement. *J. Biomech. Eng.* **2015**, *137*, 020905. [CrossRef]
65. Gupta, D.; Donnelly, C.; Reinbolt, J. Physics-Based Guidelines for Accepting Reasonable Dynamic Simulations of Movement. *IEEE Trans. -Bio-Med. Eng.* **2022**, *69*, 1194–1201. [CrossRef]
66. McGinley, J.L.; Baker, R.; Wolfe, R.; Morris, M.E. The reliability of three-dimensional kinematic gait measurements: A systematic review. *Gait Posture* **2009**, *29*, 360–369. [CrossRef]
67. Kainz, H.; Graham, D.; Edwards, J.; Walsh, H.P.J.; Maine, S.; Boyd, R.N.; Lloyd, D.G.; Modenese, L.; Carty, C.P. Reliability of four models for clinical gait analysis. *Gait Posture* **2017**, *54*, 325–331. [CrossRef]
68. Trinler, U.; Leboeuf, F.; Hollands, K.; Jones, R.; Baker, R. Estimation of muscle activation during different walking speeds with two mathematical approaches compared to surface EMG. *Gait Posture* **2018**, *64*, 266–273. [CrossRef]
69. Kainz, H.; Hoang, H.X.; Stockton, C.; Boyd, R.R.; Lloyd, D.G.; Carty, C.P. Accuracy and Reliability of Marker-Based Approaches to Scale the Pelvis, Thigh, and Shank Segments in Musculoskeletal Models. *J. Appl. Biomech.* **2017**, *33*, 354–360. [CrossRef]
70. Miller, R.H. Hill-Based Muscle Modeling. In *Handbook of Human Motion*; Müller, B., Wolf, S.I., Brueggemann, G.P., Deng, Z., McIntosh, A., Miller, F., Selbie, W.S., Eds.; Springer International Publishing: Cham, Switzerland, 2016; pp. 1–22. .203-1. [CrossRef]
71. Davoudi, M.; Salami, F.; Putz, C.; Wolf, S.I. Establishing Reference Data for Electromyographic Activity in Gait: Age and Gender Variations. *Appl. Sci.* **2025**, *15*, 3472. [CrossRef]
72. Bovi, G.; Rabuffetti, M.; Mazzoleni, P.; Ferrarin, M. A multiple-task gait analysis approach: Kinematic, kinetic and EMG reference data for healthy young and adult subjects. *Gait Posture* **2011**, *33*, 6–13. [CrossRef]
73. Schwartz, M.H.; Rozumalski, A.; Trost, J.P. The effect of walking speed on the gait of typically developing children. *J. Biomech.* **2008**, *41*, 1639–1650. [CrossRef]
74. Federolf, P.A.; Boyer, K.A.; Andriacchi, T.P. Application of principal component analysis in clinical gait research: Identification of systematic differences between healthy and medial knee-osteoarthritic gait. *J. Biomech.* **2013**, *46*, 2173–2178. [CrossRef]
75. Schweizer, K.; Cattin, P.C.; Brunner, R.; Müller, B.; Huber, C.; Romkes, J. Automatic selection of a representative trial from multiple measurements using Principle Component Analysis. *J. Biomech.* **2012**, *45*, 2306–2309. [CrossRef]
76. Pataky, T.C. One-dimensional statistical parametric mapping in Python. *Comput. Methods Biomech. Biomed. Eng.* **2012**, *15*, 295–301. [CrossRef]

77. Xu, J.; Cai, H.; Wang, Y.; Hu, Z.; Zhang, M.; Tan, Q. OpenCap-based five-times sit-to-stand analysis in older Asian women with and without sarcopenia. *Front. Aging* **2026**, *7*, 1960201. [CrossRef]
78. Moreira, L.; Figueiredo, J.; Fonseca, P.; Vilas-Boas, J.P.; Santos, C.P. Lower limb kinematic, kinetic, and EMG data from young healthy humans during walking at controlled speeds. *Sci. Data* **2021**, *8*, 103. [CrossRef]
79. Rajagopal, A.; Dembia, C.L.; DeMers, M.S.; Delp, D.D.; Hicks, J.L.; Delp, S.L. Full-Body Musculoskeletal Model for Muscle-Driven Simulation of Human Gait. *IEEE Trans. Bio-Med. Eng.* **2016**, *63*, 2068–2079. [CrossRef]
80. Bergmann, G.; Bender, A.; Graichen, F.; Dymke, J.; Rohlmann, A.; Trepczynski, A.; Heller, M.O.; Kutzner, I. Standardized loads acting in knee implants. *PLoS ONE* **2014**, *9*, e86035. [CrossRef]
81. Arnold, E.M.; Hamner, S.R.; Seth, A.; Millard, M.; Delp, S.L. How muscle fiber lengths and velocities affect muscle force generation as humans walk and run at different speeds. *J. Exp. Biol.* **2013**, *216*, 2150–2160. [CrossRef]
82. Thelen, D.G. Adjustment of Muscle Mechanics Model Parameters to Simulate Dynamic Contractions in Older Adults. *J. Biomech. Eng.* **2003**, *125*, 70–77. [CrossRef]
83. OpenSim. First-Order Activation Dynamics. 2018. Available online: https://opensimconfluence.atlassian.net/wiki/spaces/OpenSim/pages/53090590/First-Order+Activation+Dynamics (accessed on 30 October 2026).
84. Dembia, C.L.; Bianco, N.A.; Falisse, A.; Hicks, J.L.; Delp, S.L. OpenSim Moco: Musculoskeletal optimal control. *PLoS Comput. Biol.* **2020**, *16*, e1008493. [CrossRef]
85. Pizzolato, C.; Lloyd, D.G.; Sartori, M.; Ceseracciu, E.; Besier, T.F.; Fregly, B.J.; Reggiani, M. CEINMS: A toolbox to investigate the influence of different neural control solutions on the prediction of muscle excitation and joint moments during dynamic motor tasks. *J. Biomech.* **2015**, *48*, 3929–3936. [CrossRef]
86. Falisse, A.; Serrancolí, G.; Dembia, C.L.; Gillis, J.; Jonkers, I.; de Groote, F. Rapid predictive simulations with complex musculoskeletal models suggest that diverse healthy and pathological human gaits can emerge from similar control strategies. *J. R. Soc. Interface* **2019**, *16*, 20190402. [CrossRef]
87. Moissenet, F.; Chèze, L.; Dumas, R. A 3D lower limb musculoskeletal model for simultaneous estimation of musculo-tendon, joint contact, ligament and bone forces during gait. *J. Biomech.* **2014**, *47*, 50–58. [CrossRef]
88. Adouni, M.; Shirazi-Adl, A.; Shirazi, R. Computational biodynamics of human knee joint in gait: From muscle forces to cartilage stresses. *J. Biomech.* **2012**, *45*, 2149–2156. [CrossRef]
89. Bujalski, P.; Martins, J.; Stirling, L. A Monte Carlo analysis of muscle force estimation sensitivity to muscle-tendon properties using a Hill-based muscle model. *J. Biomech.* **2018**, *79*, 67–77. [CrossRef]
90. Navacchia, A.; Myers, C.A.; Rullkoetter, P.J.; Shelburne, K.B. Prediction of In Vivo Knee Joint Loads Using a Global Probabilistic Analysis. *J. Biomech. Eng.* **2016**, *138*, 4032379. [CrossRef]
91. Myers, C.A.; Laz, P.J.; Shelburne, K.B.; Davidson, B.S. A probabilistic approach to quantify the impact of uncertainty propagation in musculoskeletal simulations. *Ann. Biomed. Eng.* **2015**, *43*, 1098–1111. [CrossRef]
92. Valente, G.; Pitto, L.; Testi, D.; Seth, A.; Delp, S.L.; Stagni, R.; Viceconti, M.; Taddei, F. Are subject-specific musculoskeletal models robust to the uncertainties in parameter identification? *PLoS ONE* **2014**, *9*, e112625. [CrossRef]
93. Ackland, D.C.; Lin, Y.C.; Pandy, M.G. Sensitivity of model predictions of muscle function to changes in moment arms and muscle-tendon properties: A Monte-Carlo analysis. *J. Biomech.* **2012**, *45*, 1463–1471. [CrossRef]
94. Xiao, M.; Higginson, J. Sensitivity of estimated muscle force in forward simulation of normal walking. *J. Appl. Biomech.* **2010**, *26*, 142–149. [CrossRef]
95. Redl, C.; Gfoehler, M.; Pandy, M.G. Sensitivity of muscle force estimates to variations in muscle-tendon properties. *Hum. Mov. Sci.* **2007**, *26*, 306–319. [CrossRef]
96. Scovil, C.Y.; Ronsky, J.L. Sensitivity of a Hill-based muscle model to perturbations in model parameters. *J. Biomech.* **2006**, *39*, 2055–2063. [CrossRef]
97. Millard, M.; Uchida, T.; Seth, A.; Delp, S.L. Flexing computational muscle: Modeling and simulation of musculotendon dynamics. *J. Biomech. Eng.* **2013**, *135*, 021005. [CrossRef]
98. Charles, J.P.; Suntaxi, F.; Anderst, W.J. In vivo human lower limb muscle architecture dataset obtained using diffusion tensor imaging. *PLoS ONE* **2019**, *14*, e0223531. [CrossRef]
99. Coyler, S.; Needham, L.; Evans, M.; Wade, L.; Cosker, D.; Cazzola, D.; McGuigan, P.; Bilzon, J. Estimation of Ground Reaction Forces from markerless kinematics and comparison against measured force plate data. In *Proceedings of the 41st International Society of Biomechanics in Sports Conference*; Kipp, K., Geiser, C., Ahn, N., Eds.; Northern Michigan University: Marquette, MI, USA, 2023.
100. Karatsidis, A.; Bellusci, G.; Schepers, H.M.; de Zee, M.; Andersen, M.S.; Veltink, P.H. Estimation of Ground Reaction Forces and Moments During Gait Using Only Inertial Motion Capture. *Sensors* **2016**, *17*, 75. [CrossRef]
101. Fluit, R.; Andersen, M.S.; Kolk, S.; Verdonschot, N.; Koopman, H. Prediction of ground reaction forces and moments during various activities of daily living. *J. Biomech.* **2014**, *47*, 2321–2329. [CrossRef]

102. Wu, W.; Lee, P.V.S.; Bryant, A.L.; Galea, M.; Ackland, D.C. Subject-specific musculoskeletal modeling in the evaluation of shoulder muscle and joint function. *J. Biomech.* **2016**, *49*, 3626–3634. [CrossRef]
103. Lund, M.E.; Andersen, M.S.; de Zee, M.; Rasmussen, J. Scaling of musculoskeletal models from static and dynamic trials. *Int. Biomech.* **2015**, *2*, 1–11. [CrossRef]

Disclaimer/Publisher's Note: The statements, opinions and data contained in all publications are solely those of the individual author(s) and contributor(s) and not of MDPI and/or the editor(s). MDPI and/or the editor(s) disclaim responsibility for any injury to people or property resulting from any ideas, methods, instructions or products referred to in the content.